Zhang et al. *Zool. Res.* 2026, 47(5): 1737−1754
https://doi.org/10.24272/j.issn.2095-8137.2025.579
https://cstr.cn/32248.14.zr.2025.579

ZR | Zoological Research

Article Open Access

Fetal hypoxia causes oocyte oxidative stress damage via the Sirt3/Sod2 pathway and can be alleviated by nicotinamide mononucleotide

Lu-Yao Zhang[1,#], Ke-Xiong Liu[3,#], Ke Zhang[1,#], Xiang Qin[1], Yu-Wen Luo[2], Qing-Rui Zhuan[6], Jian Hou[2], Qi-En Yang[1,4,5,*], Yun-Peng Hou[2,*]

[1] *Key Laboratory of Adaptation and Evolution of Plateau Biota*, *Northwest Institute of Plateau Biology*, *Chinese Academy of Sciences*, *Qinghai* 810001, *China*

[2] *State Key Laboratory of Animal Biotech Breeding*, *College of Biological Sciences*, *China Agricultural University*, *Beijing* 100193, *China*

[3] *Institute of Animal Husbandry and Veterinary Medicine*, *Beijing Academy of Agriculture and Forestry Sciences*, *Beijing* 100097, *China*

[4] *University of Chinese Academy of Sciences*, *Beijing* 100049, *China*

[5] *Qinghai Key Laboratory of Animal Ecological Genomics*, *Northwest Institute of Plateau Biology*, *Chinese Academy of Sciences*, *Xining* 810001, *Qinghai*, *China*

[6] *Air Force Medical University*, *Air Force Medical Center*, *PLA*, *Beijing* 100089, *China*

ABSTRACT

Environmental hypoxia exerts detrimental effects on the reproductive capabilities of both humans and animals. A fetal hypoxia model was established in which fetal mice were kept in a high-plateau hypoxic setting from embryonic day (E) 0 to 16.5. In our previous research, we found that fetal hypoxia exposure perturbs the methylation of imprinted genes in adult sperm and causes intergenerational placental impairments in male offspring. However, the specific impacts of fetal hypoxia on the female reproductive system, particularly regarding oocyte maturation, remain poorly understood. First, we found that fetal hypoxia mice exhibited a significant reduction in the average number of pups per litter. We conducted a comprehensive analysis of the transcriptome in oocytes from the hypoxic group and investigated the metabolic alterations within the follicular microenvironment. Fetal hypoxic stress contributed to cleavage and blastocyst rate reduction and induced early apoptosis and DNA damage triggered by mitochondrial dysfunction, oxidative stress aggravation and Sirt3/Sod2 downregulation. Additionally, administration of nicotinamide mononucleotide (NMN) has been shown to prevent oocytes from mitochondrial dysfunction and developmental impairment by increasing the expression of Sirt3/Sod2 and autophagy. The number of pups per litter in fetal hypoxia mice was reduced by 57.7% compared to the control group, while NMN intervention could restore it to 73.1% of the control group. These results indicate that fetal hypoxia exposure exerts multiple potential damages to adult female reproduction, while highlighting the clinical potential of NMN supplementation as a targeted intervention to alleviate such hypoxia-associated female reproductive impairment.

Keywords: Fetal hypoxia; Oocyte development capacity; Mitochondrial dysfunction; Oxidative stress aggravation; Sirt3/Sod2; NMN

INTRODUCTION

Numerous species modify their reproductive tactics as a reaction to environmental stress (Jauniaux et al., 2006). The time of conception is a vulnerable life stage for the embryo, during which the intrauterine environment of marine may have short or long-term effects on their growth and development (Osmond & Barker, 2000). Fetal stress may bring about the maladaptive immune responses to stress that occur later in life (Bellinger et al., 2008). Diverse stressors can disrupt the balance of gonadal hormones during the critical period of fetal hypothalamic differentiation, thereby precipitating a spectrum of reproductive dysfunctions in later life (Abildgaard et al., 2014). For example, in female Drosophila, starvation stress

This is an open-access article distributed under the terms of the Creative Commons Attribution Non-Commercial License (http://creativecommons.org/licenses/by-nc/4.0/), which permits unrestricted non-commercial use, distribution, and reproduction in any medium, provided the original work is properly cited.

Copyright ©2026 Editorial Office of Zoological Research, Kunming Institute of Zoology, Chinese Academy of Sciences

Received: 18 November 2025; Accepted: 11 March 2026; Online: 18 March 2026

Foundation items: This research was funded by the Natural Science Foundation of Qinghai Province (2025-ZJ-970T), the National Natural Science Foundation of China (32400711), the National Natural Science Foundation of China (U24A201922). The Key R&D Program of the Xizang Autonomous Region (XZ202402ZY0025). The Special Research Assistant Program of the Chinese Academy of Sciences (E529051211).

[#]Authors contributed equally to this work

*Corresponding authors, Qi-En Yang, E-mail: yangqien@nwipb.cas.cn; Yunpeng Hou, E-mail: hou@cau.edu.cn

decreased the number of mature oocytes by enhancing apoptotic checkpoints and autophagy during oogenesis (Barth et al., 2011).

Oxygen is vital for most living things, especially for mammals (Hsia et al., 2013; Huang et al., 2004). High-altitude hypoxia contributes to the pathogenesis of multiple disorders, including cardiovascular diseases and metabolic abnormalities (Davies, 2003; Huang et al., 2004). Multiple studies have shown that people living above 2 500 m have a significantly higher rate of coronary heart disease, arteriosclerosis and diabetes (Giussani et al., 2014). Prenatal high-altitude hypoxia may trigger uterine or placental insults and damage fetal development. Prior research has demonstrated that abnormal levels of fetal hypoxia can result in epigenetic alterations (Simon & Keith, 2008). Although scientific data support the notion that hypoxia plays a role in fetal development (Fajersztajn & Veras, 2017), and modulates gene expression via epigenetic mechanisms (Newby et al., 2015), the specific impact of fetal hypoxia on the female reproductive system—especially on oocyte maturation and developmental competence—remains incompletely defined and controversial (Dunwoodie, 2009). Existing studies have predominantly focused on hypoxia-induced structural and functional abnormalities in ovarian somatic cells such as granulosa cells (GCs) (e.g., autophagic cell death or disrupted steroid hormone secretion) (Zhang et al., 2024a), while direct evidence linking fetal hypoxia to intrinsic oocyte defects is scarce. These processes are pivotal for oocyte maturation and developmental potential, highlighting a critical knowledge gap in the field.

Exposure to high-altitude hypoxic conditions may generate mitochondrial dysfunction and excessive accumulation of reactive oxygen species (ROS), which can potentially lead to oxidative stress in mammalian germ line cells (Okoye et al., 2023; Vargas et al., 2011). For male reproduction, exposure to hypoxia modifies metabolic processes and mitochondrial function, while also disturbing the redox balance and cell cycle progression in sperm (Vargas et al., 2011; Zhou et al., 2018). Our recent study also showed that exposure to fetal hypoxia induces DNA methylation changes in specific genes in sperm, leading to abnormal embryonic and placental development in male offspring (Zhang et al., 2025a). For ovarian GCs, hypoxia explosure maintains an excessive accumulation of ROS, resulting in mitochondrial damage in porcine, bovine and mouse models (Shiratsuki et al., 2016; Zhang et al., 2023; Zhou et al., 2018). Our earlier studies demonstrated that fetal exposure to hypoxia induced autophagic cell death of GCs through the Foxo1/PI3K/Akt signaling pathway (Zhang et al., 2023). However, little research has been done in oocytes. However, research investigating the direct effects of fetal hypoxia on oocyte biology remains limited. Regarding oocyte quality, ROS accumulation also affects mitochondrial synthesis by damaging Sirtuin family related protein activity (Dai et al., 2014). Numerous studies have shown a connection between exposure to hypoxia and the down-regulation of genes related to mitochondrial function and morphology (Guo et al., 2021; Wang et al., 2020; Zhang et al., 2019b). In addition, Sirtuin family proteins constitute a highly conserved regulatory network that modulates oocyte mitochondrial function, and their deficiency disrupts critical biological processes, ultimately leading to cell death (He et al., 2023). However, the relationships among Sirtuins, mitochondrial function and oxidative stress in oocytes from female exposed to fetal hypoxia have not been confirmed.

In the present study, we aimed to investigate the long-term impacts of fetal hypoxic stress on adult female fertility and the underlying mechanisms. We hypothesized that fetal hypoxia induces persistent oocyte defects characterized by mitochondrial dysfunction, ROS accumulation, and increased apoptosis. Furthermore, we sought to characterize metabolic perturbations in the follicular fluid and serum, which may serve as potential biomarkers or therapeutic targets for hypoxia-associated reproductive disorders. Collectively, our findings provide novel insights into the developmental origins of female reproductive dysfunction and identify potential interventions to mitigate the adverse effects of fetal hypoxia.

MATERIALS AND METHODS

Reagents

All reagents were purchased from Millipore Sigma (USA) unless otherwise stated. For details on the culture media related to oocyte and early embryo culture, please refer to Supplementary Table S2.

Ethical approval

The animal experiments were conducted in accordance with the Guide for the Care and Use of Laboratory Animals and approved by the Animal Welfare and Ethics Committee at the Northwest Institute, Chinese Academy of Sciences (AW01040202-1).

High altitude hypoxic treatment and ethics statement

8–10-week-old CD-1(ICR) mice were housed in a controlled environment with 12-hour light-dark cycles. The total number of animals included 200 female mice and 100 male mice. All mice were housed in a specific pathogen-free (SPF) animal facility under controlled environmental conditions: temperature maintained at 22–25℃, relative humidity at 50%–60%, with a 12-h light/dark cycle (lights on at 0700 h and off at 1900 h). The environmental parameters were continuously monitored using a digital recorder to ensure fluctuations within ±2℃ for temperature and ±5% for relative humidity. The control female mice were delivered by mothers who mated and became pregnant at the Central Animal Laboratory of the Institute of Zoology, China Agricultural University (50 m, 150 mmHg). The hypoxia female mice were delivered by mothers who mated and became pregnant (E0.5–16.5) at the National Field Scientific Observation and Research Station of Alpine Grassland Ecosystem, which is located in HaiBei Tibetan Autonomous Prefecture (3 300 m, 106 mmHg) (Figure 1A). To ensure consistency in environmental conditions, food and water were sourced from the same supplier. The mating experiment was conducted following the methods described in previous studies (Wang et al., 2018). Mating experiments occurred in the afternoon, and vaginal plug checks were performed the next morning; detection of a vaginal plug indicated embryonic development at approximately 0.5 days post-coitum (dpc). The hypoxia exposure stopped when mothers reached 16.5 dpc, after which they were transferred to give birth at the Animal Laboratory in China Agricultural University. Previous investigations assessing the impact of environmental transitions on maternal stress responses during pregnancy reported no significant physiological alterations in dams (Zhang et al., 2024a, 2024b). These findings indicate that brief environmental changes during transport had negligible effects on maternal physiology.

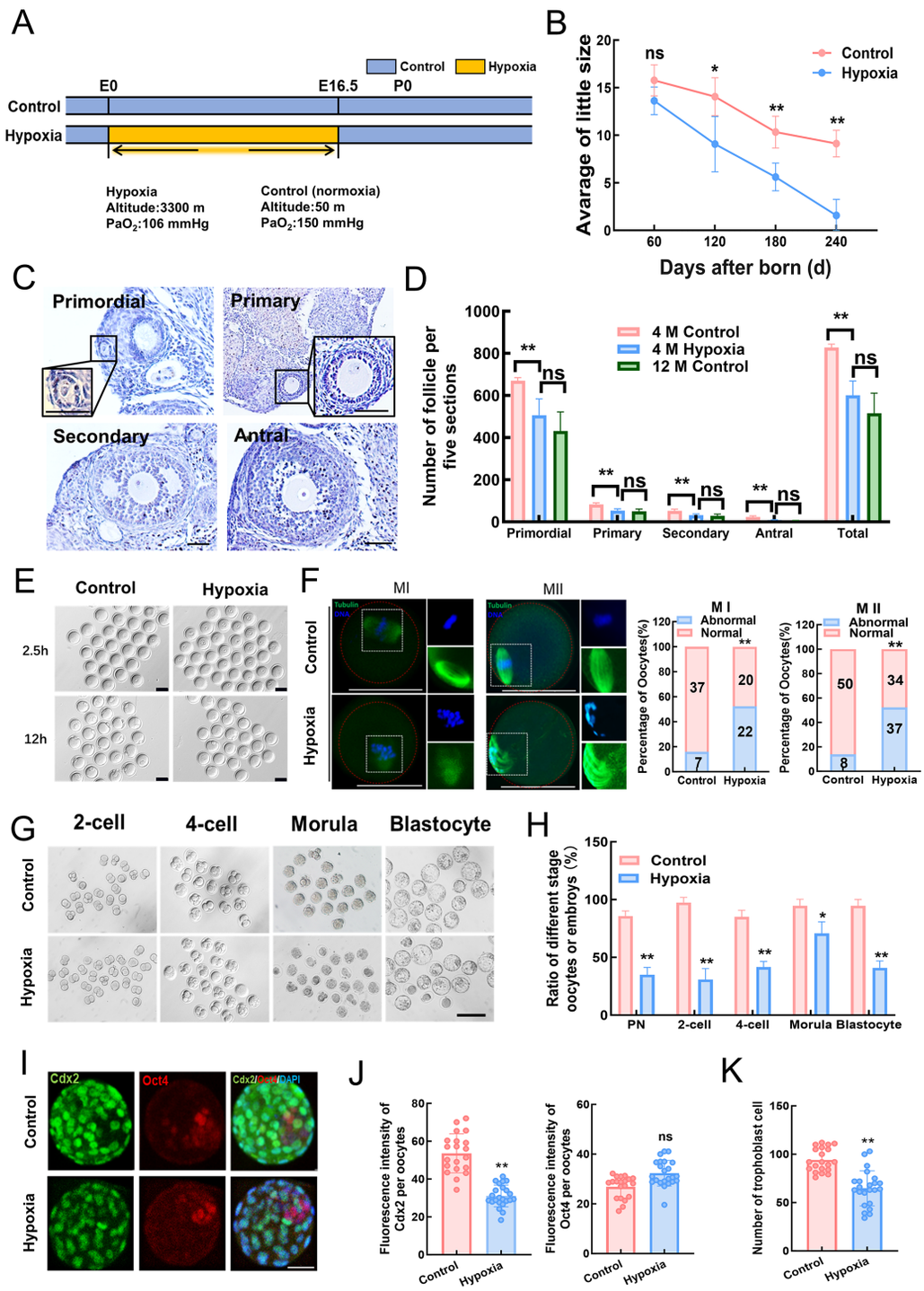


Figure 1 Effects of Hypoxia on female mice and folliculogenesis

A: A schematic representation of the treatment protocol for fetal hypoxia mice. B: Average litter size in Control (*n*=29), Hypoxia (*n*=19), all female mice were mated with control male mice. C: Representative images of ovary H&E staining. Scale bar: 50 μm. D: Quantification the number of different classes of follicles in 4-Month Control, 4-Month Hypoxia and 12-Month mice ovaries (*n*=4). E: Representative images of GVBD and PB1 in Control and Hypoxia mice oocytes. Scale bar: 50 μm. F: Control and Hypoxia MI and MII oocytes were co-stained with an α-tubulin antibody to visualize spindles (green) and with DAPI (blue) to visualize chromosomes. Scale bar: 50 μm. Quantification of Control (*n*=44) and Hypoxia (*n*=42) group MI oocytes with abnormal spindles; Quantification of Control (*n*=58) and Hypoxia (*n*=71) MII oocytes with abnormal spindles. G: Representative images of early-stage embryos developed from Control and hypoxia activated-oocytes. Scale bar: 50 μm. H: The pronucleus rate was recorded in the Control (*n*=69) and Hypoxia (*n*=66); 2-cell embryos rate was recorded in the Control (*n*=65) and Hypoxia (*n*=50); 4-cell embryos rate was recorded in the Control (*n*=45) and Hypoxia (*n*=51); the rate of morula and blastocyst formation were recorded in the Control (*n*=49) and Hypoxia (*n*=69). I: Representative images of blastocytes capacity stained by Cdx2 (Green) and Oct4 (Red) antibody in Control and Hypoxia blastocyte. Scale bar: 50 μm. J: The fluorescence intensity of Cdx2 (Green) and Oct4 (Red) were measured in Control (*n*=20) and Hypoxia (*n*=24) blastocyte. Results are presented as Mean±SD. K: Number of trophoblast cell in Control (*n*=20) and Hypoxia (*n*=23) blastocytes. ns: Not significant; *: *P*<0.05; **: *P*<0.01.

Detection of sex hormone levels

The concentration of sex hormones in the blood was assessed using an ELISA Assay Kit. A volume of 10 μm serum was added to a specialized ELISA plate coated with antibodies. Subsequently, luminescence activity was promptly measured using a luminometer (Power Wave XS2).

Ovaries H&E staining and immunofluorescence

The ovaries were fixed in a 4% paraformaldehyde (PFA) solution overnight, followed by dehydration and paraffin embedding. Sectioning was performed using a Leica microtome (RM2235, Leica, Germany), and standard procedures were used for H&E staining. Analysis was conducted using three mice in each group.

For immunofluorescence, the slices underwent deparaffinization in xylene, rehydration, and retrieval through microwave heating with Antigen Retrieval Solution buffer for 20 min. Following a one-hour blocking step with 10% donkey serum, the ovaries were stained using different primary antibodies as indicated in Table S1 for antibody dilution rates. Secondary antibodies corresponding to the primary antibodies were then applied. The fluorescence signal was analyzed by a laser scanning confocal microscope and NIS-Elements AR software.

Oocyte collection and culture

According to statistics, a total of 100 mice were used in the control group and 150 mice in the hypoxia-treated groups (including 120 mice in the hypoxia group alone and 30 mice in the hypoxia+NMN treatment group). Oocytes were obtained from 4-month-old mice. First, pregnant mare serum gonadotropin (PMSG) was administered to the mice at a dosage of 2.5–5 IU approximately 44–48 h prior. Then, the GV-stage oocytes were extracted and placed into M2 medium containing 2.5 μM milrinone. The cumulus cells were then eliminated by repeated pipetting. After microinjection or other designated treatments, the oocytes were cultured in M16 medium at 37°C, 5% CO_2 throughout the GV to MII stages.

Parthenogenetic activation

The activation medium consisted of calcium (Ca^{2+})-free HTF, to which 10 mM strontium chloride ($SrCl_2$) and 5 μg/mL cytochalasin B were added (Carbone & Tatone, 2009). Subsequently, the development of blastomeres, morulae, and blastocysts was assessed at 24-, 72-, and 96- h post-treatment, respectively. The development rate of each stage of the embryo is based on the number of oocytes initially cultured.

Oocytes immunofluorescence

After being fixed in the fixative for 40 min, the mouse oocytes were washed three times with the washing solution. Following permeation and blocking, the oocytes were incubated with the primary antibodies overnight at 4°C and subsequently incubated with the corresponding secondary antibodies. For 5-methyl cytosine (5mC) staining, denaturation was performed using hydrochloric acid before incubating with anti-5mC-FITC antibody. The fluorescence signal was analyzed by a laser scanning confocal microscope and NIS-Elements AR software.

Quantification of mitochondrial Ca^{2+} ($[Calcium]_m$) and cytosolic Ca^{2+} ($[Calcium]_c$)

The $[Calcium]_m$ and $[Calcium]_c$ were trace marked using Rhod-2AM and Fluo-4-AM (Invitrogen, U.S.) following the manufacturer's protocol, respectively. After the zona pellucida was eliminated using pronase E, oocytes were treated with 5 μM Rhod-2AM or 5 μM Fluo-4-AM in M2 medium for 30 min, followed by thorough washing with DPBS. Subsequently, they were incubated in M2 medium at 37°C, 5% CO_2 for 30 min before observation and quantification using a laser scanning confocal microscope and NIS-Elements AR software.

Investigation of mitochondrial density

Mitochondrial density was measured using Mito-tracker (Red) dye (Beyotime, China). Oocytes were incubated in M2 medium with 5 μM Mito-tracker (Red) for 40 min, washed three times with DPBS, and then observed and quantified using a laser scanning confocal microscope and NIS-Elements AR software.

Measuring ROS levels

Intracellular ROS levels were assessed using the method described in prior studies (Zhao et al., 2017). Oocytes were incubated in M2 medium with 1 mmol/L H_2DCFDA for 30 min at 37°C, followed by three washes. ROS fluorescence was observed using a fluorescence microscope with an excitation wavelength around 488 nm, and an emission wavelength around 525 nm (DP72, Olympus, Japan), and the fluorescence intensity was quantified using EZ-C1 Free-Viewer software (Nikon, Japan).

Measuring GSH levels

Intracellular glutathione (GSH) levels were determined using the methodology outlined in previous research (Zhao et al., 2017). Oocytes were incubated in M2 medium with 10 μmol/L Cell-Tracker Blue for 30 min at 37°C to measure GSH, followed by three washes. The fluorescence emitted by GSH was observed using an epifluorescence microscope (Olympus, Japan), and the fluorescence intensity measurements were conducted with the EZ-C1 Free-Viewer software.

Measurement of mitochondrial membrane potential (*Δφm*)

Mitochondrial membrane potentials (*Δφm*) of oocytes were detected by a JC-1 dye kit (Beyotime, Shanghai, China). Oocytes were treated with 10 μM JC-1 at 37°C, 5% CO_2 for 20 min, washed with DPBS, and then observed and quantified using a laser scanning confocal microscope and NIS-Elements AR software. The ratio of red to green fluorescence was reported as the *Δφm* value.

ATP content assays

Enhanced ATP Assay Kit (Beyotime, China) was used to measure the ATP content in each oocyte. Subsequently, 10 μL of the oocyte lysate was mixed with 40 μL of the kit's luciferin-luciferase substrate solution (equilibrated to room temperature in advance), and the luminescence signal was detected within 5 min of reaction initiation using an Infinite luminometer (F200, Tecan , Switzerland). The ATP levels were determined using standard curves and were adjusted according to the number of oocytes, allowing for the calculation of the average ATP content per oocyte (pmol/oocyte).

Quantitative Real-Time-PCR (qRT-PCR)

Total RNA was extracted from oocytes using the RNeasy micro-RNA isolation kit (Qiagen), followed by DNase I treatment and cDNA synthesis using Transcript-Uni Cell. The qRT-PCR reaction volume was 10 μL. qRT-PCR assays were conducted using an ABI 7500 real-time PCR instrument with

384-well plates, with all assays performed in triplicate. For validation of differentially expressed genes (DEGs) by quantitative real-time PCR (qRT-PCR), the amplification program was performed as follows: initial denaturation at 95°C for 30 s, followed by 40 cycles of denaturation at 95°C for 5 s and annealing/extension at 60°C for 34 s; a melting curve analysis (95°C for 15 s, 60°C for 1 min, 95°C for 15 s) was conducted to confirm the specificity of PCR products. The relative gene expression levels were determined using the threshold cycle (CT) method, calculated as $2^{-\Delta\Delta CT}$. The primers utilized are listed in Supplementary Table S3.

The mRNA expression of *Tet1* and *Tet2*

The mRNA expression levels of *Tet1* and *Tet2* were also examined via qRT-PCR assays. We collected embryos from the hypoxia and control groups at different developmental stages to perform a series of experiments, including microRNA extraction (DP42, TIANGEN, China) and cDNA library construction. The relative gene expression levels were determined using the threshold cycle (CT) value, calculated as target gene (*Tet1/Tet2*)/ *β-Actin*.

RNA sequencing

We performed expression profiling on collections of 15 denuded GV-oocytes, extracting RNA with the RNeasy Micro Kit from Qiagen. Following this, cDNA synthesis and amplification were carried out utilizing the Nu-Gen Ovation RNA-seq System V2. The resultant SPIA cDNA was employed to construct sequencing libraries using the Tru-Seq DNA Sample Preparation Kit (low-throughput protocol). After performing equimolar pooling, the libraries underwent sequencing for 50 cycles on the Illumina Hi-Seq 2000 platform, with base calling executed by RTA v.1.13.48. Later, demultiplexing and the generation of FastQ files were achieved through bcl2fastq software (v.1.8.3).

Data Analysis

Analysis of differential expression between two groups was performed utilizing the DESeq2 R package (v.1.20.0). This package applies statistical techniques to detect differential expression in digital gene expression datasets, relying on a model that follows the negative binomial distribution. P-values generated were corrected for multiple comparisons using the Benjamini-Hochberg method to regulate the false discovery rate. Genes identified with an adjusted *P*-value<0.05 and $\log_2$(fold change)>1, as indicated by DESeq2, were deemed differentially expressed.

Gene Ontology (GO) and Kyoto Encyclopedia of Genes and Genomes (KEGG) enrichment analysis

GO and KEGG enrichment analysis of differentially expressed genes (DEGs) was conducted using the ClusterProfiler R package (v.4.3.2), with adjustments made to correct for gene length bias. GO terms or KEGG pathways with an adjusted P-value<0.05 were deemed significantly enriched among the DEGs. The KEGG database (www.genome.jp/kegg/) provides comprehensive information on high-level biological processes.

Alternative Splicing (AS) analysis

AS is a crucial mechanism for regulating gene expression and protein variability. The rMATS software (v.3.2.5) was employed to analyze AS events.

PPI analysis of differentially expressed genes

The protein-protein interaction (PPI) analysis of differentially expressed genes was conducted using the STRING database (v.12.0), which encompasses both known and predicted protein-protein interactions.

Annexin V staining

The oocytes were washed and resuspended in pre-chilled DPBS. A mixture of annexin V-FITC, PI staining solution, and binding buffer was then added for a 10 min incubation in darkness. Subsequently, the fluorescence intensity of Annexin V was assessed using EZ-C1 Free-Viewer to identify early apoptotic cells.

Follicular fluid and serum metabolite profiles

Follicular fluid was collected from mouse ovarian follicles: five ovaries per group were placed in sterile 35 mm Petri dishes, and surface follicles were punctured under a stereomicroscope with a 1 mL syringe. Extruded fluid (120 μL per group) was immediately transferred to 1.5 mL sterile centrifuge tubes, rapidly frozen in liquid nitrogen, and stored at –80°C. Serum samples (150–200 μL per group) were collected from mice via cardiac puncture and frozen using the same protocol as that for follicular fluid.

Metabolite samples were analyzed following the method of Liu et al. (2023). Quantification of metabolites was conducted utilizing the SCIEX UPLC system (Exion LC, SCIEX, Concord, NH) alongside a quadrupole-time-of-flight mass spectrometer (QTOF MS; Triple TOF 5600+, SCIEX, USA). Metabolites were confidently identified by three-tiered validation: Retention time (RT) deviation ≤ ±0.05 min vs. standards; Parent ion mass error ≤ ±5 ppm; MS/MS fragmentation matching score≥ 80% (vs. HMDB, METLIN, in-house library; SCIEX OS v.1.4).

The method was validated using quality control (QC) samples pooled from all experimental samples, with precision characterized by an intra-day relative standard deviation (RSD) of retention time (RT)≤2.0% and peak area≤5.0% (6 replicates) as well as an inter-day RSD of peak area≤7.0% (3 consecutive days), accuracy verified by a recovery rate of 85.3–108.7% (RSD≤4.5%) through the spiking of 20 standard metabolites (e.g., nicotinamide, NMN, glutathione), and stability demonstrated by an RSD≤6.0% for peak area/RT in QC samples stored at –80°C for 0, 7, 14, and 30 days. Differential metabolites were chosen using VIP≥1.0 (OPLS-DA) and $|\log_2(\text{fold change})|>1.0$. Metabolic pathway enrichment was analyzed via KEGG and MetaboAnalyst 5.0 (adjusted *P*<0.05).

Transmission Electron Microscope

Samples containing 30–40 oocytes were acquired and reseeded in 4-well plates. They were then treated with 500μL of 3% glutaraldehyde per well. Subsequently, oocytes were subjected to post-fixation in 1% osmium tetroxide, followed by dehydration in acetone, infiltration with Epox 812, and embedding. Methylene blue was used to stain semithin sections, while ultrathin sections were created using a diamond knife and subsequently stained with uranyl acetate and lead citrate prior to examination under a JEM-1400-FLASH Transmission Electron Microscope.

***In vitro* and *in vivo* dose of NMN treatment**

***In vitro* treatment**: The NMN dose used in the present study was determined based on (Miao et al., 2021, 2022; Noh et al., 2026; Song et al., 2022). Studies across multiple species have shown that the optimal concentration of NMN for treating oocytes *in vitro* ranges from 10 to 100 μM. Therefore, we used GV oocytes from control and hypoxia mice were cultured in M16 medium with or without 10, 40 and 100 μM NMN for

14–16 h at 37°C under 5% CO_2. After *in vitro* maturation, the rate of PBE was assessed, and oocytes were subjected to analyses of $\Delta\Psi m$ and ROS levels.

***In vivo* treatment**: The NMN dose used in the present study was determined based on (Miao et al., 2020). NMN was dissolved in sterile PBS to prepare a stock solution of 100 mg/mL. Mice were administered NMN via intraperitoneal injection using a 1 mL syringe with a 20G needle. Each mouse received 0.1 mL of the NMN stock solution per day, which corresponds to a dose of 200 mg/kg body weight per day. Control mice were injected with an equal volume of sterile PBS. The treatment was continued for 14 consecutive days (from postnatal day 21 to day 35).

Statistical analyses

All experiments were independently repeated at least three times. Data are presented as mean±standard deviation (SD), unless otherwise specified. Statistical analyses were performed using SPSS (v.19.0). Statistical comparisons were made using analysis of variance (ANOVA) or Student's *t*-tests. $P<0.05$ was considered statistically significant.

RESULTS

Fetal hypoxia impairs fertility capacity in adults

To ascertain the potential effects of high-altitude-hypoxia during fetal development on adult fertility, we established a model to simulate fetal hypoxic stress (Figure 1A). Short-term exposure to high altitude hypoxic environment induced significant changes in female reproductive function and survival rate (Figure 1B; Supplementary Figure S1A). The litter size of hypoxic mice decreased rapidly from 2 to 8 months of age, with few offspring at 8 months (Figure 1B). In 4-month-old hypoxic mice, the concentrations of FSH, LH and estradiol showed variation trends similar to those in aged mice (Figures S1B–G). Based on these observations, we concluded that hypoxia impairs the growth and fertility of female mice exposed to hypoxia. To investigate its impact on ovarian development, we examined folliculogenesis in 4-month-old hypoxic mice. The results showed that similar to aged mice, the total count of follicles across all developmental stages significantly decreased in the hypoxic mice (Figures 1C, D; Supplementary Table S5).

Fetal hypoxia impairs oocyte developmental capacity in adults

Meiotic maturation starts with germinal vesicle breakdown (GVBD) and the first polar body extrusion (PBE) of the oocyte, which is utilized to evaluate oocyte maturation quality. As expected, more hypoxic oocytes were blocked at the GV stage, and the rate of PBE was significantly decreased in hypoxia oocytes 12 h (Figure 1E; Supplementary Figures S2A, B). Subsequently, we found that the percentage of spindle abnormalities increased in MI and MII hypoxic oocytes (Figure 1F). The mRNA expression of marker genes for oocyte maturation, including *Bmp15* and *Gdf9*, visibly decreased in hypoxic oocytes (Supplementary Figure S2C). Together, these findings indicate that fetal hypoxia affected the oocyte quality and the meiotic process in adults. Meanwhile, the developmental capacity of the oocytes was assessed. The rates of pronucleus formation, cleavage (2-cell embryo) and blastocyst formation of the hypoxia oocytes were lower than those of the control (Figures 1G, H; Supplementary Table S5). Furthermore, fetal hypoxia downregulated the DNA 5hmC level in blastocysts (Supplementary Figures S2D–E), which may caused by the decrease in *Tet1* expression (Supplementary Figures S2F–I). Early blastocyst capacity assessed by $Cdx2^+$ and $Oct4^+$ staining showed that $Cdx2^+$ cells were significantly lower in the hypoxia group (Figures 1I–K). Additionally, the mRNA expression of some maternal effect factors remarkably declined in hypoxic oocytes (Supplementary Figure S2J). In conclusion, fetal hypoxia impairs the oocyte quality and further damages embryonic development.

Identification of key effectors in hypoxic oocytes by RNA-seq transcriptome analysis

We analyzed the transcriptome of ovulated oocytes from control and hypoxic mice to identify genetic and pathway effects. The results showed 843 upregulated and 1 312 downregulated differentially expressed genes (DEGs) in hypoxic oocytes compared to controls (Figure 2A; Supplementary Table S6). Furthermore, the common genes among the top 30 in fold change and P-value of downregulated genes were verified by qRT-PCR (Figures 2B, C). GO analysis showed that the DEGs were enriched in oocyte maturation progress, mitochondrial assembly, autophagy, and nucleotide metabolic processes (Figure 2D; Supplementary Figure S3A). GSEA demonstrated that downregulated genes were related to oxidative phosphorylation, the TCA cycle, Sirt3 and cell development pathways (Figure 2E). PPI analysis and multiple AS analysis also revealed that fetal hypoxia had an adverse effect on oocyte maturation, oocyte aging and embryogenesis (Supplementary Figures S3B–D).

Fetal hypoxia stress leads to mitochondrial dysfunction and oxidative stress aggravation in oocytes

Transcriptome data showed that fetal hypoxia affected oocyte mitochondrial function and interfered with oxidative phosphorylation and the TCA cycle. Therefore, we evaluated the mitochondrial function and structure, the results suggested that the abnormal structure of mitochondria increased and the mitochondrial density decreased significantly in hypoxic oocytes (Figures 3A–C; Supplementary Figures S4A–E). Additionally, the expression of genes related to mitochondrial fusion (*Opa1*, *Mfn1* and *Mfn2*), fission (*Drp1*), and mitochondrial function related genes (*Ndufs1*, *Ndufs3*, *Ndufs4*, *Sirt3*, and *Sdhb*) was abnormally regulated in hypoxic oocytes (Figures 3D, E). As expected, the MMP and ATP levels were decreased in hypoxic oocytes (Figures 3F–H; Supplementary Figure S4F; Supplementary Table S5). Collectively, these findings indicate that mitochondrial function and dynamics are compromised in oocytes from the hypoxia group.

Fetal hypoxia aggravates oxidative stress, DNA damage, impaired autophagy and apoptosis in oocytes

RNA-seq data showed that apoptosis related genes were expressed abnormally (Figure 2D). At the same time, previous research found that mitochondrial dysfunction might lead to oxidative stress and apoptosis (Zhang et al., 2019a). The ROS level increased and GSH level decreased markedly in hypoxic oocytes (Figure 3I; Supplementary Figure S5A), and the expression of antioxidant related genes was significantly downregulated (Supplementary Figure S5B). Our previous study indicated that mitochondrial dysfunction and oxidative stress might lead to intracellular calcium disorder (Zhang et al., 2020). Fluorescence measurements indicated that much

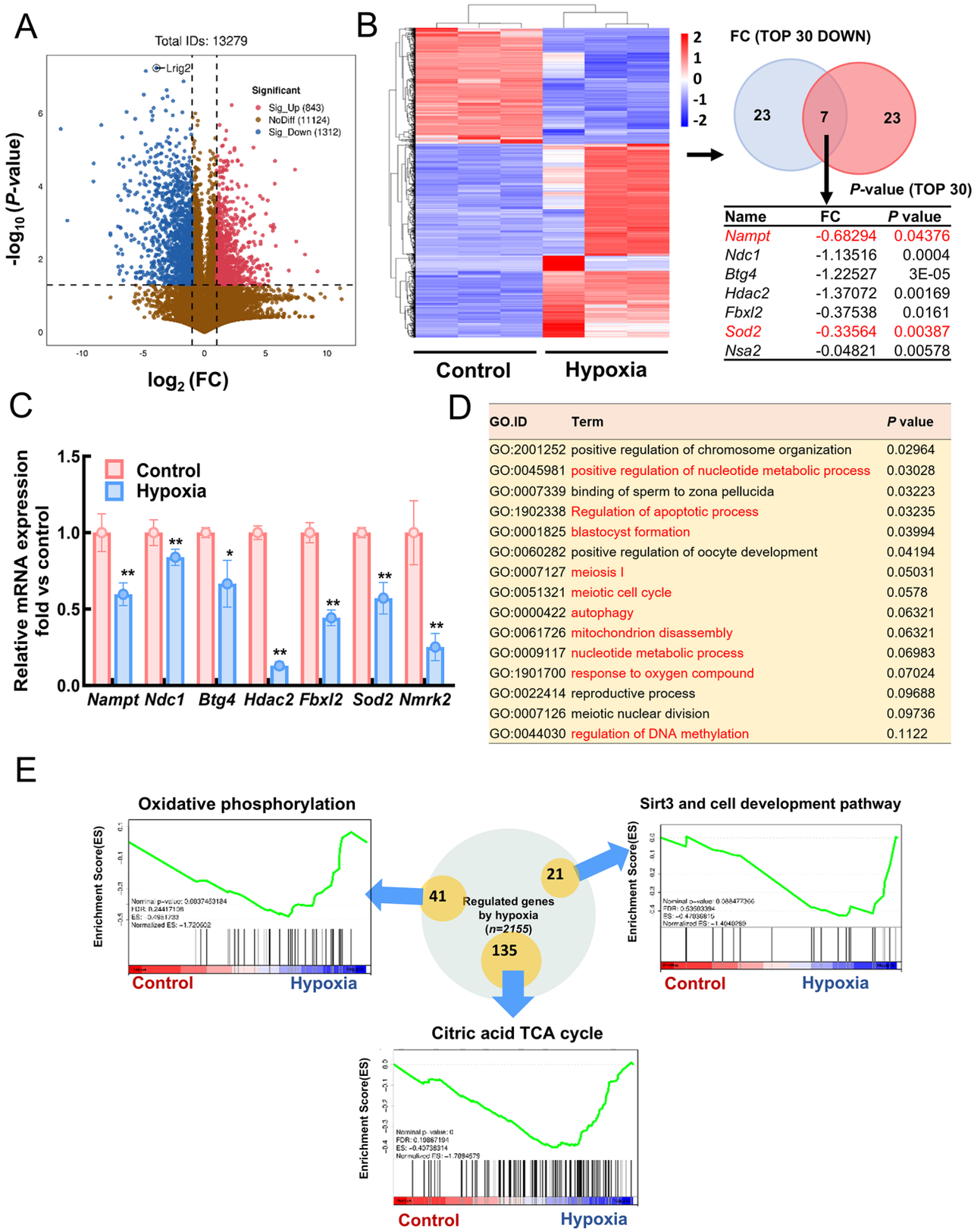


Figure 2 RNA-seq data reveal alterations in gene expression under both control and hypoxia

A: Volcano plot illustrating the DEGs between Control and Hypoxia groups; Red: upregulated genes; Green: downregulated genes. B: Heatmap depicting DEGs in Control and Hypoxia oocytes. C: qRT-PCR to detect expressions of *Nampt*, *Ndc1*, *Btg4*, *Hdac2*, *Fbxl2*, *Sod2* and *Nmrk2* in oocytes. D: Table of Go enrichment of DEGs in Control and Hypoxia. E: GSEA enrichment of DEGs in Control and Hypoxia. Results are presented as Mean±SD. *: $P < 0.05$; **: $P < 0.01$.

stronger $[Ca^{2+}]_m$ and $[Ca^{2+}]_c$ signals appeared in hypoxic oocytes (Supplementary Figures S5C–E). The DNA damage and apoptosis remarkably increased in hypoxia oocytes (Figure 3J; Supplementary Figures S6A–C); meanwhile,

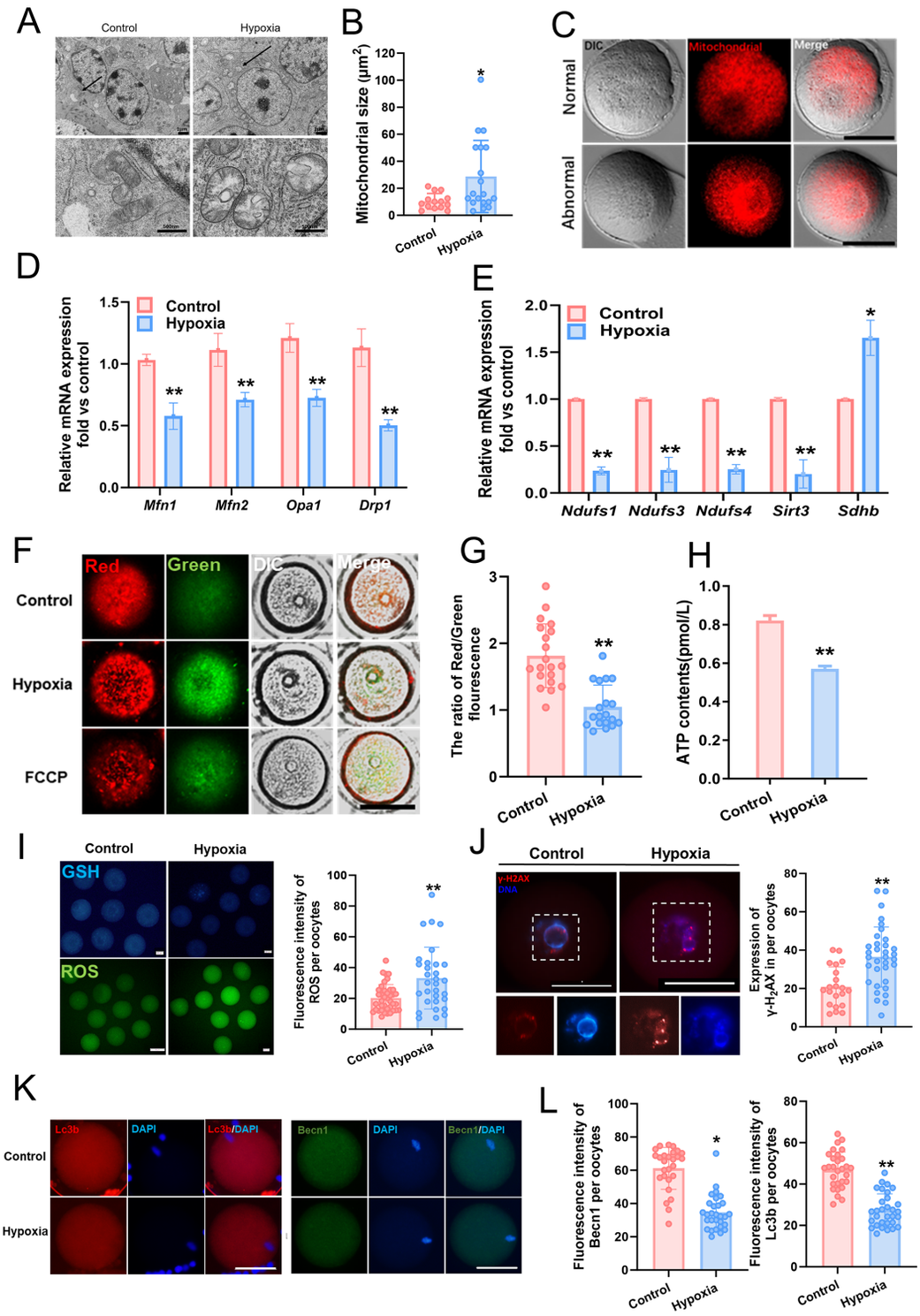


Figure 3 Mitochondrial Function and autophagy are damaged in hypoxia oocytes

A, B: The TEM imaging of oocytes mitochondrial structures. Scale bar: 1 μm. Mitochondrial sizes collected in GV oocytes for Control and Hypoxia. C: Representative images of normal and abnormal mitochondrial distribution. Scale bar, 50 μm. D: Expression of *Opa1*, *Mfn1*, *Mfn2*, and *Drp1* were examined by qRT-PCR in Control and Hypoxia GV oocytes. E: The expression of *Ndufs1*, *Ndufs3*, *Ndufs4*, *Sirt3* and *Sdhb* were examined by qRT-PCR in Control and Hypoxia GV oocytes. F, G: Mitochondrial membrane potential (*Δφm*) in Control and Hypoxia GV oocytes. Scale bar: 50 μm. The ratio of red to green fluorescence intensity was calculated in Control (*n*=44) and Hypoxia (*n*=43) GV oocytes. H: ATP concentrations of individual GV oocytes in Control and Hypoxia groups (*n*=40). I: Representative images of ROS levels and GSH levels in Control and Hypoxia GV oocytes. Scale bar: 50 μm. The fluorescence intensity of ROS signals was measured in Control (*n*=39) and Hypoxia (*n*=24) GV oocytes. J: Representative images of DNA damage stained by γ-H_2AX antibody in Control and Hypoxia GV oocytes. Scale bar: 20 μm. The fluorescent signal intensity of γ-H_2AX were counted in Control (*n*=21) and Hypoxia (*n*=34) GV oocytes. K: Representative images of Lc3b and Becn1 in Control and Hypoxia oocytes. Scale bar: 20 μm. L: The fluorescence intensity of Lc3b, Becn1 were counted in Control (Lc3b: *n*=30; Becn1: *n*=27) and Hypoxia (Lc3b: *n*=31; Becn1: *n*=30) oocytes. Results are presented as mean±SD. *: $P < 0.05$; **: $P < 0.01$.

apoptosis related genes or proteins were also expressed abnormally in hypoxic oocytes (Figures S6D, E). Additionally, statistical results suggested that Becn1 (Green) and Lc3b (Red) declined in hypoxic oocytes and qRT-PCR results were similar to immunofluorescence results (Figures 3K–L; Supplementary Figures S6F). Our data showed that fetal hypoxia aggravates oxidative stress, DNA damage, impaired autophagy and apoptosis in adult oocytes.

Sirt3 overexpression could partially improve oocyte quality and retard oxidative stress in fetal hypoxic mice

Combining RNA-seq data, we attempted to figure out the molecular mechanisms and key regulatory genes in fetal hypoxic mouse oocytes. GSEA and PPI of DEGs were enriched in Sirt family genes, such as *Sirt3* (Figures 2E and 4A). Immunofluorescence results showed that Sirt3 declined in hypoxic oocytes (Figure 4B). To confirm the effect of Sirt3, we microinjected hypoxic oocytes to overexpress Sirt3 (Figures 4C–D; Supplementary Figures S6G). *Sirt3* overexpression in hypoxia oocytes could retard oxidative stress and partly recover mitochondrial function (Figures 4E–K). The apoptosis and autophagic levels also improved dramatically (Figures 4L–M; Supplementary Figures S6H). Additionally, PPI of DEGs suggested that Sod2 might interact with Sirt3 (Figure 4A). Then we examined the expression of Sod2 after *Sirt3* overexpression. Sod2 protein expression was partially restored in *Sirt3*-overexpressed hypoxic oocytes (Figure 4N). Our data showed that *Sirt3* overexpression could improve oocyte quality in fetal hypoxic mice.

NMN supplementation could partially improve oocyte quality and the Sirt3/Sod2 pathway in fetal hypoxic mice

To investigate the interaction between oocytes and their microenvironment, we conducted widely targeted metabolomic analysis of mouse follicular fluid (Supplementary Figure S7A; Supplementary Table S7). A total of 742 metabolites were identified, with 175 upregulated and 114 downregulated (Figure 5A). Nicotinamide mononucleotide (NMN) metabolism, oxidative phosphorylation, and tricarboxylic acid (TCA) cycle pathways were the core significantly enriched pathways (adjusted P<0.05). Among the metabolites involved, NMN levels were significantly downregulated, the content of α-ketoglutarate was decreased, and the concentration of reduced glutathione (GSH) was reduced, all of which showed characteristic changes associated with fetal hypoxia. Subsequent co-analysis of RNA-seq data and follicular fluid metabolites showed co-enrichment of DEGs and DEMs in 25 KEGG pathways (Figure 5B), including oxidative phosphorylation and NMN metabolism. Furthermore, notable differences in DEMs within the NMN metabolic pathway were observed (Figures 5C, D; Supplementary Figure S7B). Given that the sirtuin family participates in NMN metabolism, we then detected NMN metabolism-related genes such as *Sirt1*, *Sirt2*, *Sirt3*, *Nampt*, *Nmnat1*, *Nmnat2*, *Nmnat3*, and *Naprt*, qRT-PCR results indicated that *Sirt3* mRNA expression decreased remarkably (Figure 5E). The above results suggested that NMN deficiency may be the key regulator of Sirt3 decline in hypoxic oocytes.

To verify our hypothesis, hypoxic oocytes were treated with NMN. As shown in Figure 6A and S8A, 40μM NMN was chosen as the optimal dose and oocyte maturation regulated genes *Bmp15* and *Gdf9* were upregulated after NMN treatment (Supplementary Figures S8B, C). Subsequently, the western blot and immunofluorescence staining results indicated that Sirt3 and acetylated-Sod2 had significant changes after NMN treatment (Figures 6B, C; Supplementary Figures S8D, E). NMN treatment of hypoxic oocytes could improve mitochondrial density (Figure 6D; Supplementary Figure S8F). Meanwhile, the ATP and MMP levels recovered significantly, and the mitochondrial function related genes ameliorated after NMN supplementation (Supplementary Figures S8G–I). Besides, NMN treatment in hypoxic oocytes could retard oxidative stress (Figures 6E, F; Supplementary Figure S8J) and apoptosis (Figure 6G). Autophagic marker proteins Becn1 (green), Lc3b (red), and autophagy-related genes (*Atg5*, *Atg7*, *Becn1*, *Lc3b*, and *Sqstm1*) also ameliorated via NMN addition (Figures 6H–K). In summary, our data indicated that NMN supplementation could moderate the Sirt3/Sod2 pathway to partially improve oocyte quality in fetal hypoxic mice.

NMN partially enhanced fertility and ovarian function of fetal hypoxic mice

In addition to changes in the oocyte microenvironment, we also focused on systemic metabolic abnormalities induced by fetal hypoxia, with a particular commitment to elucidating the physiological crosstalk between follicular fluid metabolism and systemic circulation. By exploring the "follicular microenvironment-systemic circulation" metabolic axis, we aimed to identify key common regulators that modulate both the oocyte microenvironment and systemic metabolic homeostasis in the fetal hypoxia group (Supplementary Table S8). Therefore, we performed a metabolome test on serum and found that serum Nicotinamide-N-Oxide and Nicotinamide content also decreased in fetal hypoxic mice similar to the follicular fluid metabolome (Figures 7A; Supplementary Figure S9). We investigated whether NMN could enhance fertility and ovarian function in mice exposed to fetal hypoxia. Mice subjected to hypoxia were administered either PBS or NMN via daily injections for 14 consecutive days (from postnatal day 21 to day 35) and were subsequently mated with male mice following the treatment period (Figure 7B; Supplementary Table S4). Secondary and antral follicles showed a significant amelioration after NMN treatment in hypoxic ovaries (Figures 7C, D). Immunofluorescence staining analysis identified increased EdU^+ cells and declined $TUNEL^+$ cells after NMN treatment, suggesting improved cell proliferation and apoptosis improvement in fetal hypoxic ovaries (Figures 7E, F; Supplementary Figures S10A, B). The pups per litter of hypoxic mice recovered to a similar level as the control after NMN treatment (Figures 7G, H). Additionally, the amino acid content in E19.5 embryo serum and the birth weight recovered after NMN treatment (Figure 7I; Supplementary Figure S10C); furthermore, the physical indicators also returned to normal at 3 weeks and 2 months (Figure 7J; Supplementary Figure S10D). Both results suggested that their offsprings' development partially recovered after NMN supplementation (Figure 8).

DISCUSSION

In this study, we examined the effects of fetal hypoxic stress on female fertility in adults and attempted to elucidate the related mechanisms. Fetal hypoxic stress induces long-term hypo-fertility in adult females, a phenotype consistent with the "developmental origins of health and disease" (DOHaD) theory (Osmond & Barker, 2000). This reduced fertility reflects

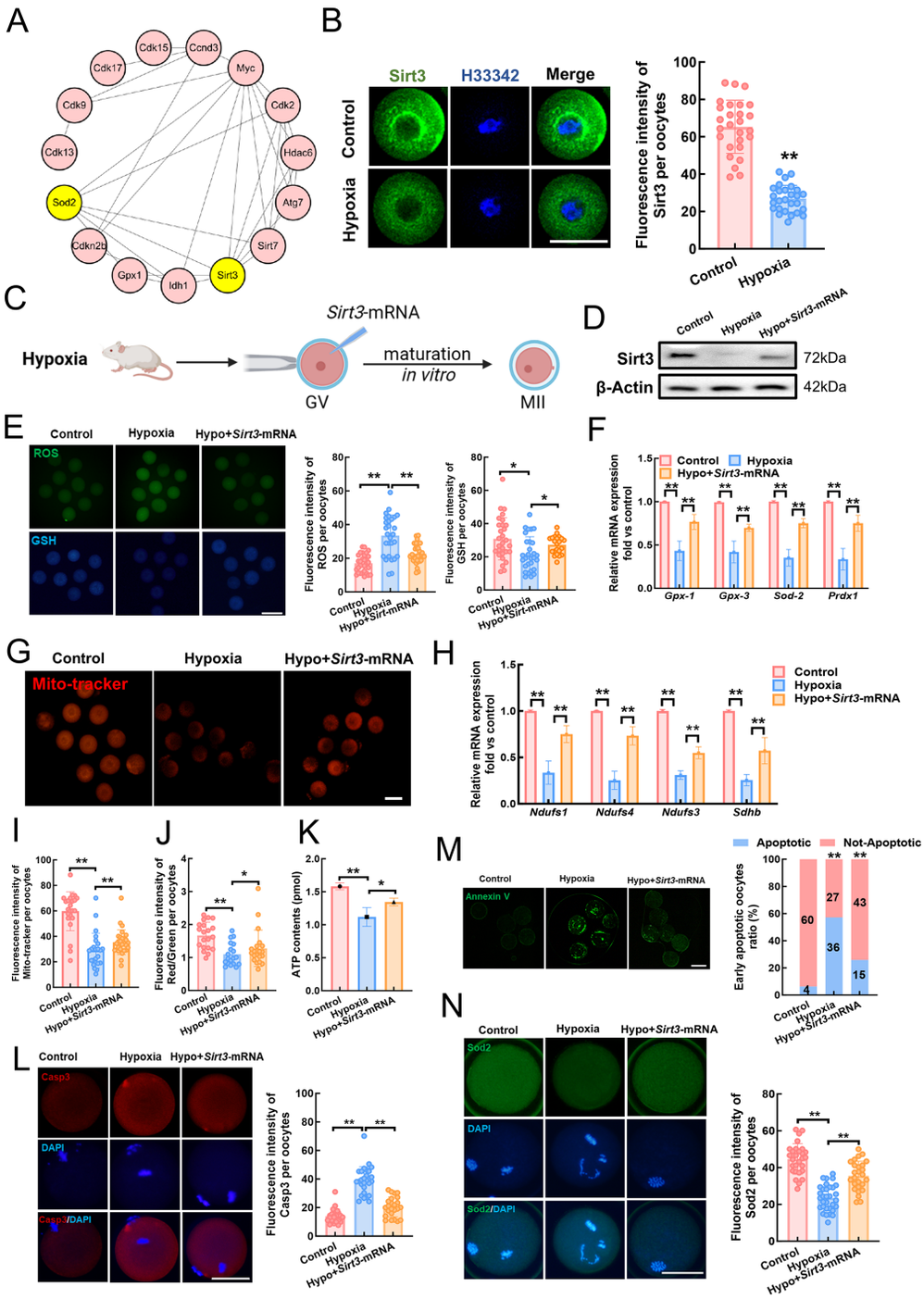


Figure 4 ***Sirt3*** **overexpress could ameliorate mitochondrial dysfunction and oxidative stress damage in hypoxia mice oocytes.**

A: PPI interacted with Sirt pathway signal in DEGs. B: Representative images of Sirt3 protein expression levels detected in Control (*n*=27) and Hypoxia (*n*=27) GV oocytes. Scale bar: 50 μm. C: The model of overexpression *Sirt3*-mRNA microinjected in Hypoxia oocytes. D: Sirt3 protein expression in Control, Hypoxia and Hypoxia+*Sirt3*-mRNA GV oocytes. E: Representative images of ROS and GSH levels in Control, Hypoxia and Hypoxia+ *Sirt3*-mRNA GV oocytes. Scale bar, 50 μm; Control (ROS: *n*=30, GSH: *n*=29), Hypoxia (ROS: *n*=28, GSH: *n*=29) and Hypoxia+*Sirt3*-mRNA (ROS: *n* =30, GSH: *n*=22) GV oocytes. F: The expression of *Gpx-1*, *Gpx-3*, *Sod-2* and *Prdx1* were examined by qRT-PCR in Control, Hypoxia and Hypoxia+*Sirt3*-mRNA GV oocytes. G: Representative images of mitochondrial density in Control, Hypoxia and Hypoxia+ *Sirt3*-mRNA GV oocytes. Scale bar: 50 μm. H: The expression of *Ndufs1*, *Ndufs3*, *Ndufs4* and *Sdhb* were examined by qRT-PCR in Control, Hypoxia and Hypoxia+ *Sirt3*-mRNA GV oocytes. I: The fluorescence intensity of Mito-tracker in Control (*n*=24), Hypoxia (*n*=26) and Hypoxia+*Sirt3*-mRNA (*n*=29) GV oocytes. J: Mitochondrial membrane potential (*Δφm*) in Control (*n*=20), Hypoxia (*n*=19) and Hypoxia+*Sirt3*-mRNA (*n*=21) GV oocytes. K: ATP concentrations of individual oocytes in Control, Hypoxia and Hypoxia+*Sirt3*-mRNA GV oocytes (*n*=40). L: Representative images of Caspase 3 protein expression levels in Control (*n*=25), Hypoxia (*n*=28) and Hypoxia+*Sirt3*-mRNA (*n*=24) MII oocytes. Scale bar: 50 μm. M: Representative images of early apoptosis detected by Annexin V staining in Control (*n*=64), Hypoxia (*n*=63) and Hypoxia+*Sirt3*-mRNA (*n*=58) MII oocytes. Scale bar: 50 μm. N: Representative images of Sod2 protein expression levels in Control (*n*=28), Hypoxia (*n*=32) and Hypoxia+*Sirt3*-mRNA (*n*=26) MII oocytes. Scale bar: 50 μm. Results are presented as mean±SD. ns: Not significant; *: *P*<0.05; **: *P*<0.01.

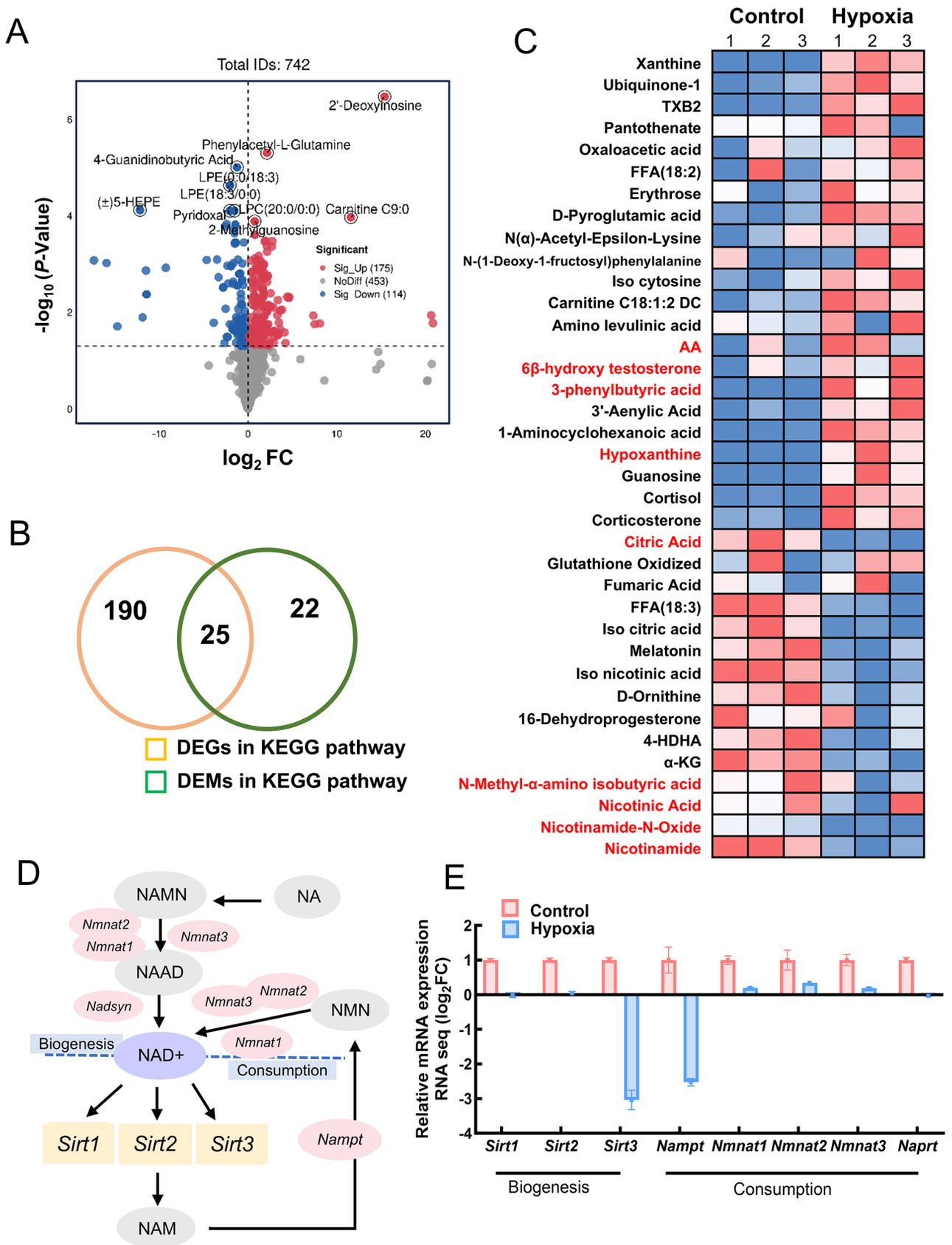


Figure 5 Metabolome analysis of follicular fluid in control and hypoxia mice

A: Volcano plot illustrating the DEMs between Control and Hypoxia groups follicular fluid; Red: upregulated; Green: downregulated. B: DEGs in KEGG pathway shared with differential metabolites in KEGG pathway. C: Heatmap of DEMs in Control and Hypoxia follicular fluid. D: Metabolome and transcriptome association analysis of metabolic pathways. E: qRT-PCR of genes showed in the NMN biogenesis and consumption in Control and Hypoxia follicular fluid.

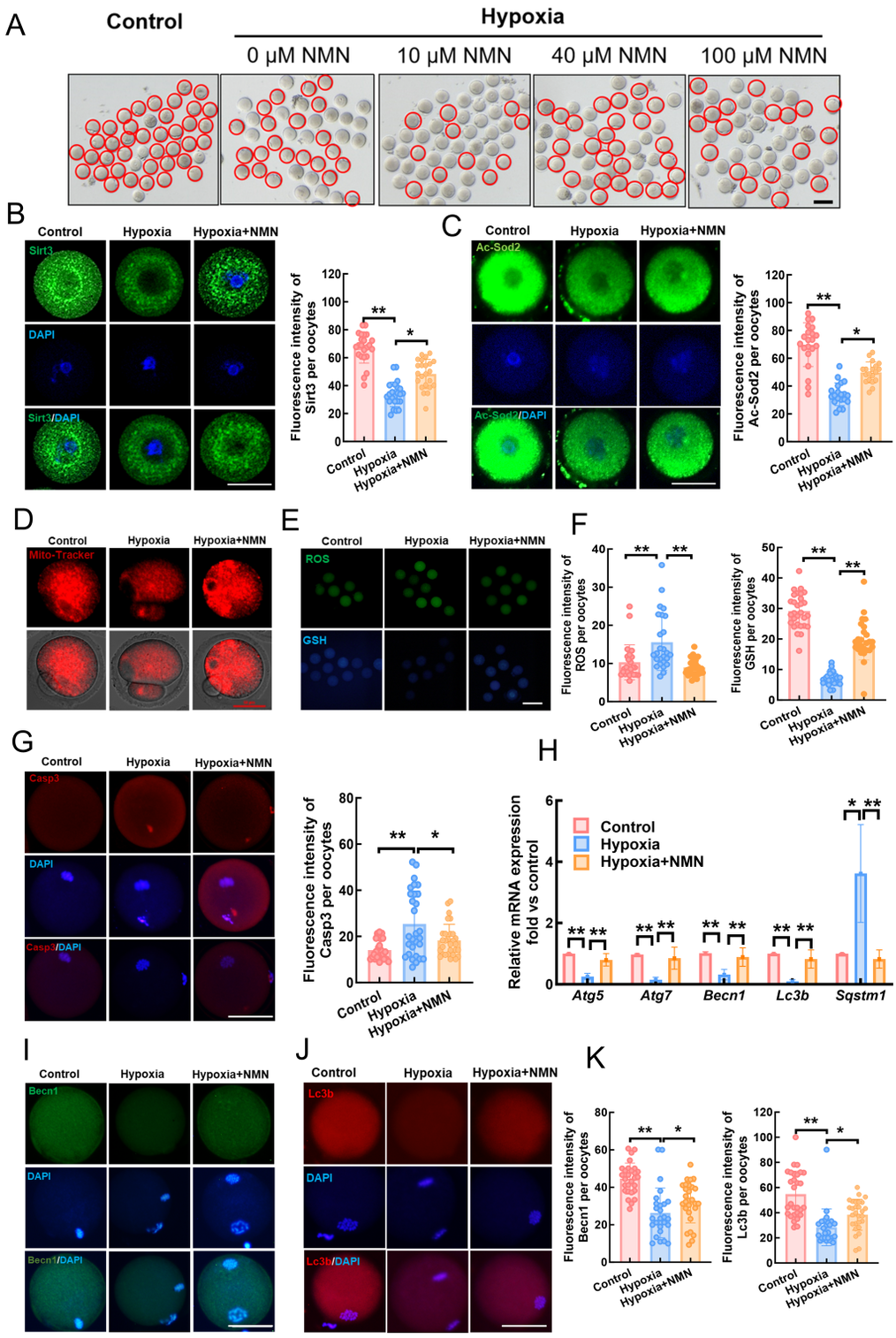


Figure 6 NMN supplement *in vitro* could improve quality of hypoxia oocytes

A: Representative images of PB1 after 12 h extrusion oocytes in Control and Hypoxia mice. Scale bar: 50 μm. B: Representative images of Sirt3 protein expression levels in Control (*n*=23), Hypoxia (*n*=23) and Hypoxia+NMN (*n*=23) GV oocytes. Scale bar: 50 μm. C: Representative images of Acetyl-Sod2 protein expression levels in Control (*n*=21), Hypoxia (*n*=20) and Hypoxia+NMN (*n*=19) GV oocytes. Scale bar: 50 μm. D: Representative images of mitochondrial density in Control, Hypoxia and Hypoxia + NMN GV oocytes. Scale bar: 50 μm. E, F: Representative images of ROS and GSH levels in control, Hypoxia and Hypoxia+NMN GV oocytes. Scale bar: 50 μm. Control (ROS: *n*=26, GSH: *n*=29), Hypoxia (ROS: *n*=44, GSH: *n*=24) and Hypoxia+NMN (ROS: *n*=29, GSH: *n*=26). G: Representative images of Caspase3 protein expression levels in Control (*n*=25), Hypoxia (*n*=29) and Hypoxia+NMN (*n*=29) MII oocytes. Scale bar: 50 μm. H: The mRNA expression of *Atg5*, *Atg7*, *Becn1*, *Lc3b* and *Sqstm1* were examined by qRT-PCR in Control, Hypoxia and Hypoxia+NMN MII oocytes. I, K: Representative images of Becn1(green) and Lc3b (red) protein expression levels in Control, Hypoxia and Hypoxia+ NMN MII oocytes. Scale bar: 50 μm; Control (Becn1: *n*=28, Lc3b: *n*=29), Hypoxia (Becn1: *n*=26, Lc3b: *n*=25) and Hypoxia+NMN (Becn1: *n*=28, Lc3b: *n*=28). Results are presented as mean±SD. ns: Not significant; *: P<0.05; **: P < 0.01.

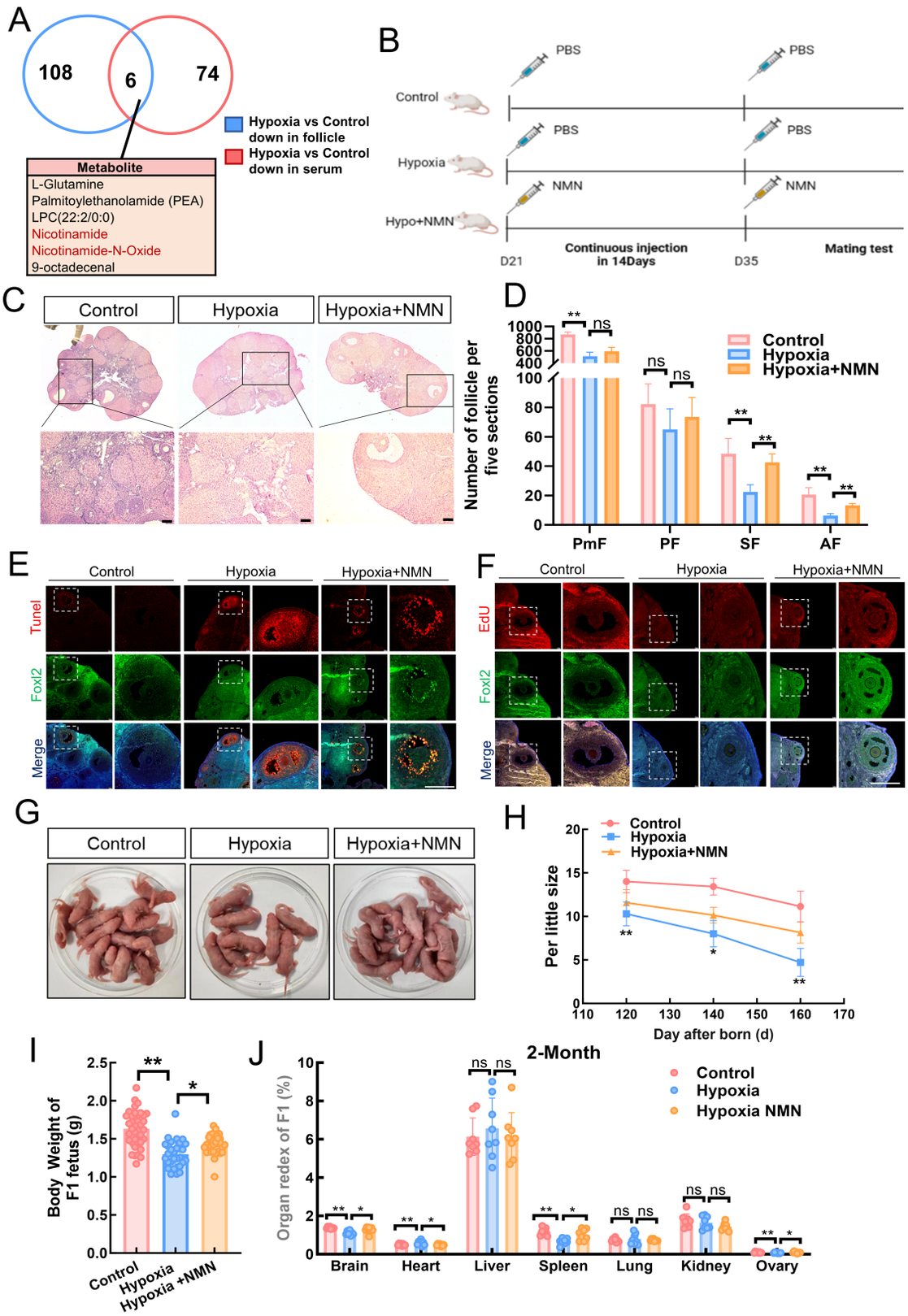


Figure 7 NMN supplement *in vivo* could improve reproductive capacity of hypoxia mice

A: Common differential metabolites in serum and follicular fluid metabolome. B: Schematic diagram of the processing scheme in NMN treatment *in vivo*. C: Representative images of ovary sections. Scale bars: 50μm. D: Total number of different classes of follicles and different classes of follicles in Control, Hypoxia and Hypoxia+NMN ovaries (n=4). E, F: Representative images of follicle sections in Tunel (Red)/Foxl2 (Green) and EdU (Red)/Foxl2 (Green) via immunofluorescence staining (n=6). Scale bar: 50μm. G: Representative images of litter size in Control, Hypoxia and Hypoxia+NMN groups. H: Litter size statistics in Control, Hypoxia and Hypoxia+NMN groups (n=7). I: Body weight of fetus in Control (n=39), Hypoxia (n=30) and Hypoxia+NMN (n =33). J: Organ index of brain, heart, liver, spleen, lung, kidney and ovary in 2 Month F1 mice of Control, Hypoxia and Hypoxia+NMN groups (n=8). Results are presented as mean±SD. ns: Not significant; *: $P < 0.05$; **: $P < 0.01$.

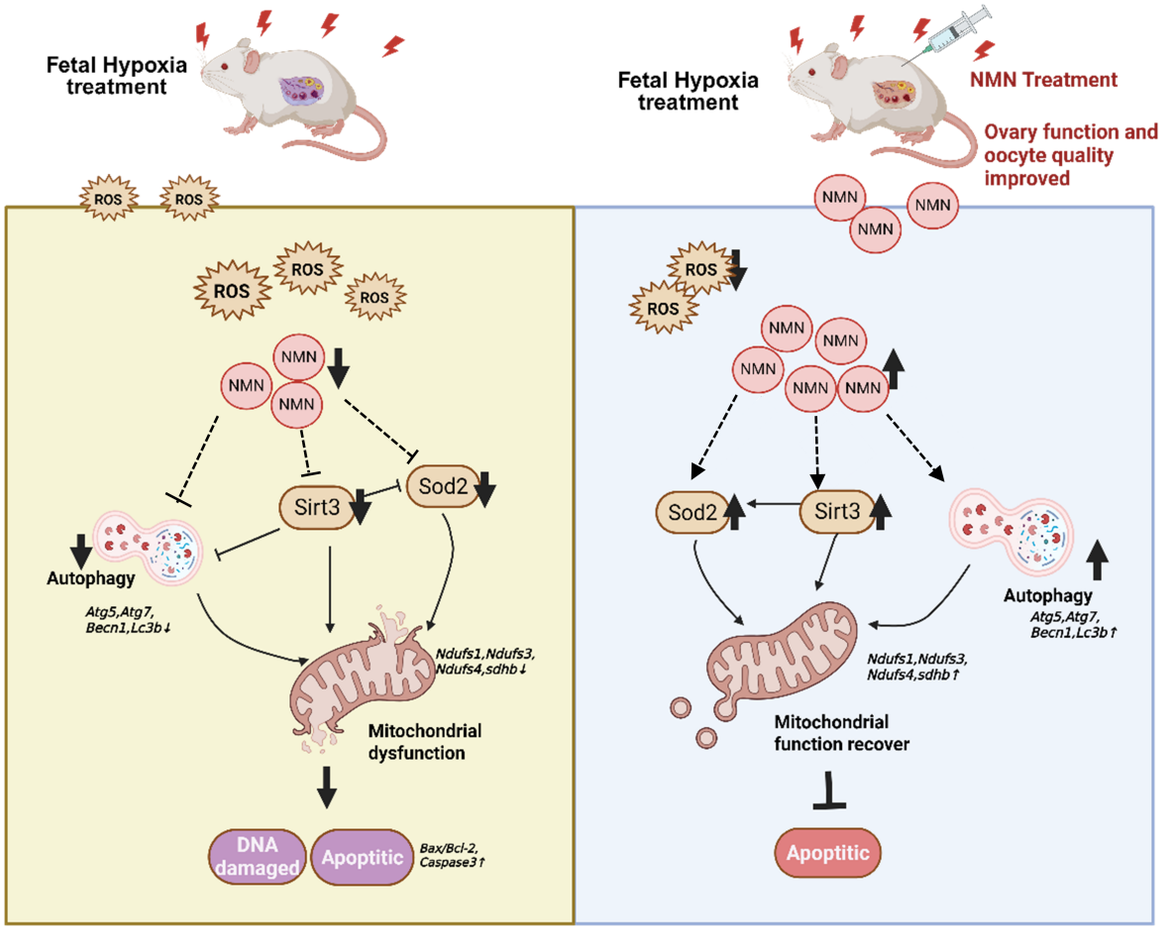


Figure 8 Fetal hypoxia causes oocyte oxidative stress damage via Sirt3/sod2 pathway and could alleviated by nicotinamide mononucleotide

accelerated ovarian aging—evidenced by follicular depletion and sex hormone dysregulation similar to that in aged mice—with core mechanisms involving Sirt3/Sod2 pathway downregulation and follicular fluid NMN deficiency that disrupt oocyte mitochondrial homeostasis and embryonic developmental competence (Figure 8).

Hypoxia is a critically important environmental factor that influences health and disease in both human and animal populations inhabiting high-altitude regions (Julian & Moore, 2019; Simonson et al., 2010). In our study, we found that hypoxia seriously damages the reproductive performance of female mice resulting in similarities to aged mice. For male reproduction, chronic hypoxia exposure led to declined plasma testosterone levels (Alcantara-Zapata et al., 2022), and dilation of the blood vessels was noted throughout the testis (Fahim et al., 1980). According to our data, the levels of LH, FSH and E2 were obviously downregulated in fetal hypoxia ovaries, which parallels findings in aged mice. The number of follicles available in the ovary, also called ovarian reserve, is the primary determinant of female reproduction (Mclaughlin & Mciver, 2009). Notably, these ovarian and endocrine perturbations (reduced follicle count and dysregulated sex hormones) may exert secondary effects on oocyte quality: FSH and LH are essential for maintaining a favorable follicular microenvironment (e.g., nutrient supply, cytokine balance) required for oocyte maturation, while estradiol directly modulates mitochondrial function and redox balance in oocytes (Tatone et al., 2015). Thus, the depleted ovarian reserve and impaired HPG axis function in hypoxia-exposed females may further exacerbate intrinsic oocyte defects by disrupting supportive signaling pathways. Hypoxia leads to a decrease in sperm count and may be associated with an increase in germ cell apoptosis(Jankovic Velickovic & Stefanovic, 2014). A recent study shows that high-altitude induced hypoxia may alter sex hormone levels, such as gonadotropin and steroid hormones through metabolic regulation (Marcouiller et al., 2021). The hypothalamus-pituitary-gonadal axis (HPG), known as the key regulator of LH and FSH, is indispensable for maintaining ovarian function and folliculogenesis (Liu et al., 2023). Our findings regarding accelerated follicular depletion in fetal hypoxia ovaries agree with rapid decline in fecundity observed in fetal hypoxia mice.

The maintenance of ovarian and oocyte function constitutes two necessary aspects of female reproduction. We found that fetal hypoxia affected oocyte quality in adults. Meiotic and embryonic developmental competencies rely on a proper oocyte maturation (Babayev & Seli, 2015). The main role of CDX2 in embryonic development is to maintain embryonic growth, induce cell differentiation, and promote organ formation (Lau et al., 2023). Our immunofluorescence staining results suggested that the number of $CDX2^{+}$ cells in hypoxic blastocysts declined remarkably. Combined with the qRT-PCR analysis of maternal effect factors, we found that embryonic developmental competency was impaired in the hypoxia group. DNA methylation levels (5mC) are modulated by DNA methyltransferases (*Dnmt1*, *Dnmt3a*, and *Dnmt3b*) and DNA demethylases (*Tet1* and *Tet2*) (Gao et al., 2012). The reduced 5mC levels in our results indicated that fetal hypoxia had

changed the status of DNA methylation in oocytes, suggesting changes in epigenetic modifications. Given that primordial follicles (the source of adult oocytes) are established during fetal development (Mclaughlin & Mciver, 2009), this critical window makes oocytes highly susceptible to hypoxic programming. These epigenetic changes (e.g., reduced 5mC and downregulated Tet1; Figure S2D–K) may persist into adulthood, directly impairing oocyte meiotic progression and mitochondrial biogenesis independently of postnatal endocrine status—consistent with our previous finding that fetal hypoxia induces germ cell epigenetic modifications (Zhang et al., 2025a). Our GSEA and GO analyses suggested that oxidative phosphorylation, Sirt3, and cell development, the mitochondrial respiratory chain and oocyte developmental capacity were affected in hypoxic oocytes. Under physiological conditions, the mitochondrial respiratory chain serves as the primary source of ROS, and a balance is maintained between ROS production and ATP levels in oocytes (Zhang et al., 2019a). Hypoxia-induced mitochondrial respiratory chain dysfunction leads to excessive ROS leakage, while the downregulation of antioxidant genes (*Gpx-1*, *Gpx-4*, *Prdx1*) in hypoxic oocytes further exacerbates redox imbalance—creating a "ROS overload-mitochondrial damage" positive feedback loop. Statistical analysis revealed significant positive correlations between ROS levels and notable negative correlations with sperm parameters, including count and motility (Ata-Abadi et al., 2020). Our findings suggest that oocytes from fetal hypoxia mice exhibit reduced antioxidant capacity, potentially resulting in increased ROS accumulation and apoptosis. Hypoxia exposure alters metabolism and mitochondrial function and also disrupts the redox balance in cells (Soltani et al., 2019)

Sirtuins constitute a versatile protein family, each member residing in distinct subcellular compartments and influencing a broad spectrum of cellular processes, such as metabolism regulation and epigenetic modification (Ji et al., 2022; Vo et al., 2023). Specifically, SIRT3, SIRT4, and SIRT5, which are localized within the mitochondrial matrix, have been identified as key mediators linking oxidative stress to metabolic pathways (Ji et al., 2022; Kumar & Lombard, 2015). In the context of female reproduction, multiple studies have demonstrated that reduced SIRT1 expression is associated with diminished ovarian reserve, both physiologically and pathologically (Di Emidio et al., 2021; Tatone et al., 2015). Additionally, SIRT1 has been shown to regulate granulosa cell (GC) proliferation and apoptosis, while SIRT3 promotes luteinization (Tatone et al., 2018). Modulating the activity of sirtuins biochemically has revealed the roles of SIRT1, SIRT2, SIRT3, and SIRT6 in enhancing the developmental competence of oocytes cultured or matured *in vitro*, as observed in both human and animal models. High expression of Sirt1 and Sirt2 can significantly improve the quality of mammalian aging oocytes (Han et al., 2015; Zhang et al., 2015). Furthermore, particular focus has been placed on the Sirt3/Sod2 interaction with oxidative stress to regulate mitochondrial redox reactions and autophagy (Pi et al., 2015; Zhang et al., 2022). Notably, both ROS overaccumulation and Sirt3 downregulation—identified through multi-omics analysis—serve as key drivers of mitochondrial damage in oocytes. Consistent with numerous studies on oocytes (Mani et al., 2024), Sirt3 plays a pivotal role in regulating mitochondrial homeostasis and preserving oocyte developmental competence: by stabilizing mitochondrial membrane potential and mitigating ROS-mediated DNA damage, it effectively suppresses mitochondria-dependent apoptotic pathways (e.g., Caspase-3 activation), thereby reducing the early apoptosis rate of oocytes and safeguarding their normal development (Kordowitzki, 2024). Furthermore, a study on human oocytes demonstrated that Sirt3-mediated mitochondrial function directly predicts implantation success (Soltani et al., 2019; Zhao et al., 2016) , and insufficient Sirt3 expression reduces blastocyst formation rate and $Cdx2^+$ trophoblast cell numbers—phenotypes that align with our fetal hypoxia model. This consistency highlights clinical relevance, as Cdx2 is essential for trophoblast differentiation and placental development (Lau et al., 2023), linking fetal hypoxia to embryonic implantation failure—a major cause of infertility.

Fetal hypoxia can lead to sustained stress through metabolic alterations (Wu et al., 2023). Under hypoxic conditions, mitochondria undergo fission and adopt a fragmented morphology, potentially to facilitate mitophagy, maintain ROS levels within physiological limits, and preserve cellular integrity by reducing respiratory activity (Shiratsuki et al., 2016). This metabolic reprogramming leads to an excessive buildup of ROS, which facilitates the continuous activation of the transcription factor HIF-1α (Wu et al., 2023). Hypoxia led to abnormal oxidative phosphorylation, thereby affecting the TCA cycle and its metabolic products (Fuller & Kim, 2021). Previous studies confirmed that hypoxia compromises the function of the uterus or placenta and induces epigenetic alterations that affect fetal development. Our metabolomics data analysis demonstrated that the DEMs in plasma and follicular fluid were conspicuously concentrated in the TCA cycle and NMN metabolism. In the co-analysis of the two metabolomics datasets, we noted a significant downregulation of NMN in both groups. These results provide a novel perspective on the formation of "hypoxic memory" from the fetal period to adulthood is presented, suggesting a potential approach to enhance fertility in women exposed to hypoxic conditions.

NMN serves as a precursor of NAD^+, which is a crucial coenzyme in the tricarboxylic acid cycle, facilitating the metabolism of sugars, fats, and amino acids and participating in the energy synthesis (Liu et al., 2021). NMN has been gaining increasing attention as a promising anti-aging and antioxidant product via improving mitochondrial function (Okabe et al., 2019). NMN is primarily distributed in the nucleus, mitochondria, and cytoplasm. In humans, it can also be detected in placental tissue and various body fluids, including blood and urine (Nadeeshani et al., 2022). Recent investigations have suggested that the addition of NMN helps to alleviate the decline in fertility observed in aged mice by improving oocyte quality (Miao et al., 2021; Zhang et al., 2023). Analysis of metabolomic data from follicular fluid and serum revealed a significant downregulation of NMN synthesis, with Sirt1-3 playing crucial catalytic roles in this process. Subsequent findings indicated a notable downregulation of Sirt3/Sod2 in hypoxic oocytes. As a direct precursor of NAD^+, NMN enters oocytes via Slc12a8 transporters localized on the plasma membrane (Soma & Lalam, 2022), and is rapidly converted to NAD^+ by intracellular nicotinamide mononucleotide adenylyl transferases (Nmnat1/2/3)—with Nmnat3 specifically localized in mitochondria to ensure localized NAD^+ replenishment (Okabe et al., 2019). The elevated NAD^+ levels directly activate Sirt3, a class III histone deacetylase (HDAC) dependent on NAD^+ as

a co-substrate: NAD^+ binds to the catalytic domain of Sirt3, inducing a conformational change that enhances its deacetylase activity. Sirt3 then translocates to the mitochondrial matrix, where it specifically targets the lysine 68 (K68) residue of Sod2 for deacetylation (Dai et al., 2014). By replenishing NMN, we not only restore NAD^+ biosynthesis to reactivate Sirt3-mediated deacetylation of Sod2 and autophagic regulators but also break the "hypoxia-NAD^+ depletion-Sirt3 inactivation-oxidative stress" vicious cycle. Notably, our *in vitro* and *in vivo* NMN interventions provide indirect evidence for the synergistic roles of intrinsic oocyte defects and systemic endocrine perturbations: *in vitro* NMN treatment (without endocrine modification) partially restored oocyte mitochondrial function and maturation (Figure 6), confirming reversible intrinsic defects, while *in vivo* administration concurrently improved follicle counts, litter size, fetal weight and postnatal development of the fetus (Figure 7), validating NMN's dual targeting of both pathways. This multi-targeted molecular mechanism explains why NMN can effectively improve oocyte maturation, embryonic developmental competence, and litter size in fetal hypoxia-exposed mice. In addition, NMN serves not only as an antioxidant for protecting mitochondria but also as an important regulatory factor in aging (Nadeeshani et al., 2022; Soma & Lalam, 2022). The decrease in NMN levels caused by embryonic hypoxia not only results in reproductive aging and oocyte anomalies but may also be a primary contributor to reduced mouse survival rates. However, our experimental design is limited by the lack of continuous tracking of the survival rate of hypoxic embryonic mice following NMN treatment. We solely investigated offspring production, offspring development, and ovarian function after NMN treatment.

Notably, NMN's regulation of oocyte quality is not dependent on a single pathway. Our transcriptomic KEGG enrichment analysis identified the phosphatidylinositol signaling system (mmu04070, P=0.001059) (Zhang et al., 2024c), MAPK signaling pathway (mmu04010, P=0.008704) (Zhang et al., 2025b), and cell cycle pathway (mmu04110, P=0.004917) as potential targets of NMN, each contributing to oocyte function maintenance by regulating anti-apoptosis, stress balance, or meiotic progression (Ramírez-Martín et al., 2025). These three pathways synergistically support NMN's protective effects from distinct dimensions, further confirming the complexity and pleiotropy of its regulatory mechanisms. Consistent with our observation that NMN only partially rescues oocyte defects induced by fetal hypoxia, these findings suggest additional uncharacterized pathways may be involved in this process, highlighting the need for more systematic mechanistic dissection in future studies.

To summarize, our results uncover a novel phenomenon indicating that fetal hypoxic stress could potentially trigger various female reproductive issues. We acknowledge that the current study does not quantitatively dissect the exact proportion of contributions from direct oocyte programming versus secondary endocrine effects—a limitation we plan to address in future research via oocyte transfer experiments (transferring hypoxia-exposed GV oocytes into normal recipient mice) to isolate intrinsic defects from systemic perturbations. Future research should conduct a more thorough investigation into the impacts of fetal hypoxic stress on both human and animal reproduction.

CONCLUSION

Our findings illustrated that fetal hypoxia had a serious influence on female reproductive function in adults. Fetal hypoxia reduced the GVBD and PB1 rates and disrupted the meiotic spindle morphology in oocytes. Oocytes from hypoxic fetuses exhibited early apoptosis and DNA damage triggered by mitochondrial dysfunction and Sirt3/Sod2 downregulation. NMN administration could recover the quality and fertility of hypoxic oocytes via the Sirt3/Sod2 pathway. NMN played an important role in hypoxic female reproductive function and oocyte developmental potency (Figure 8).

DATA AVAILABILITY

All data generated or analyzed during this study are included in this published article and its supplementary information files. The raw datasets of oocytes RNA-seq were deposited into National Center for Biotechnology Information (NCBI Bio Project ID：PRJNA1277786) database, the Genome Sequence Archive (GSA) of the China National Center for Bioinformation (CRA025649). Science Data Bank (Transcriptomics DOI: 10.57760/sciencedb. j00139.00263; Metabolome Database DOI: 10.57760/sciencedb. j00139.00263).

SUPPLEMENTARY DATA

Additional file 1. Table S1-S3 and Figure. S1-S10

Table S1 Antibody information

Table S2 Table of mediums used for oocyte and early embryo culture

Table S3 Oligonucleotide primer sequences used for quantitative real-time PCR

Table S4 Blood physiology and biochemistry in serum

CONFLICTS OF INTEREST

The authors declare that they have no competing interests.

AUTHORS' CONTRIBUTIONS

Z.L.Y. and L.K.X. performed the principal experiments and contributed to the original draft. Z.K. and L.Y.W. assisted in conception, data analysis and interpretation. L.Y.W. and Z.Q.R. made a concentrated effort to finish the animal experiments. Z.L.Y., Z.K. and Q.X. provided bioinformatics analysis and technical assistance. H.J., Y.Q.E. and H.Y.P. contributed to conception and project administration. All authors read and approved the final version of the manuscript.

REFERENCES

Abildgaard A, Lund S, Hougaard KS. 2014. Chronic high-fat diet increases acute neuroendocrine stress response independently of prenatal dexamethasone treatment in male rats. *Acta Neuropsychiatrica*, **26**(1): 8–18.

Alcantara-Zapata DE, Llanos AJ, Nazzal C. 2022. High altitude exposure affects male reproductive parameters: could it also affect the prostate?. *Biology of Reproduction*, **106**(3): 385–396.

Ata-Abadi NS, Mowla SJ, Aboutalebi F, et al. 2020. Hypoxia-related long noncoding RNAs are associated with varicocele-related male infertility. *PLoS One*, **15**(4): e0232357.

Babayev E, Seli E. 2015. Oocyte mitochondrial function and reproduction. *Current Opinion in Obstetrics & Gynecology*, **27**(3): 175–181.

Barth JMI, Szabad J, Hafen E, et al. 2011. Autophagy in Drosophila ovaries is induced by starvation and is required for oogenesis. *Cell Death & Differentiation*, **18**(6): 915–924.

Bellinger DL, Lubahn C, Lorton D. 2008. Retracted: maternal and early life stress effects on immune function: relevance to immunotoxicology. *Journal of Immunotoxicology*, **5**(4): 419–444.

Carbone MC, Tatone C. 2009. Alterations in the protein kinase C signaling

activated by a parthenogenetic agent in oocytes from reproductively old mice. *Molecular Reproduction and Development*, **76**(2): 122–131.

Dai SH, Chen T, Wang YH, et al. 2014. Sirt3 attenuates hydrogen peroxide-induced oxidative stress through the preservation of mitochondrial function in HT22 cells. *International Journal of Molecular Medicine*, **34**(4): 1159–1168.

Davies MJ. 2003. Singlet oxygen-mediated damage to proteins and its consequences. *Biochemical and Biophysical Research Communications*, **305**(3): 761–770.

Di Emidio G, Falone S, Artini PG, et al. 2021. Mitochondrial sirtuins in reproduction. *Antioxidants*, **10**(7): 1047.

Dunwoodie SL. 2009. The role of hypoxia in development of the mammalian embryo. *Developmental Cell*, **17**(6): 755–773.

Fahim MS, Messiha FS, Girgis SM. 1980. Effect of acute and chronic simulated high altitude on male reproduction and testosterone level. *Archives of Andrology*, **4**(3): 217–219.

Fajersztajn L, Veras MM. 2017. Hypoxia: from placental development to fetal programming. *Birth Defects Research*, **109**(17): 1377–1385.

Fuller GG, Kim JK. 2021. Compartmentalization and metabolic regulation of glycolysis. *Journal of Cell Science*, **134**(20): jcs258469.

Gao C, Han HB, Tian XZ, et al. 2012. Melatonin promotes embryonic development and reduces reactive oxygen species in vitrified mouse 2-cell embryos. *Journal of Pineal Research*, **52**(3): 305–311.

Giussani DA, Niu YG, Herrera EA, et al. 2014. Heart disease link to fetal hypoxia and oxidative stress. In: Zhang LB, Ducsay CA. Advances in Fetal and Neonatal Physiology. New York: Springer, 77–87.

Guo HJ, Ding H, Yan YX, et al. 2021. Intermittent hypoxia-induced autophagy via AMPK/mTOR signaling pathway attenuates endothelial apoptosis and dysfunction in vitro. *Sleep and Breathing*, **25**(4): 1859–1865.

Han LS, Ge J, Zhang L, et al. 2015. Sirt6 depletion causes spindle defects and chromosome misalignment during meiosis of mouse oocyte. *Scientific Reports*, **5**(1): 15366.

He HN, Wang JL, Mou XM, et al. 2023. Selective autophagic degradation of ACLY (ATP citrate lyase) maintains citrate homeostasis and promotes oocyte maturation. *Autophagy*, **19**(1): 163–179.

Hsia CCW, Schmitz A, Lambertz M, et al. 2013. Evolution of air breathing: oxygen homeostasis and the transitions from water to land and sky. *Comprehensive Physiology*, **3**(2): 849–915.

Huang STJ, Vo KCT, Lyell DJ, et al. 2004. Developmental response to hypoxia. *The FASEB Journal*, **18**(12): 1348–1365.

Jankovic Velickovic L, Stefanovic V. 2014. Hypoxia and spermatogenesis. *International Urology and Nephrology*, **46**(5): 887–894.

Jauniaux E, Poston L, Burton GJ. 2006. Placental-related diseases of pregnancy: involvement of oxidative stress and implications in human evolution. *Human Reproduction Update*, **12**(6): 747–755.

Ji ZJ, Liu GH, Qu J. 2022. Mitochondrial sirtuins, metabolism, and aging. *Journal of Genetics and Genomics*, **49**(4): 287–298.

Julian CG, Moore LG. 2019. Human genetic adaptation to high altitude: evidence from the andes. *Genes*, **10**(2): 150.

Kordowitzki P. 2024. Elucidating the role of sirtuin 3 in mammalian oocyte aging. *Cells*, **13**(18): 1592.

Kumar S, Lombard DB. 2015. Mitochondrial sirtuins and their relationships with metabolic disease and cancer. *Antioxidants & Redox Signaling*, **22**(12): 1060–1077.

Lau KYC, Amadei G, Zernicka-Goetz M. 2023. Assembly of complete mouse embryo models from embryonic and induced stem cell types in vitro. *Nature Protocols*, **18**(12): 3662–3689.

Liu KX, Zhang LY, Qi Q, et al. 2023. Growth hormone treatment improves the development of follicles and oocytes in prepubertal lambs. *Journal of Ovarian Research*, **16**(1): 132.

Liu Y, Luo CT, Li T, et al. 2021. Reduced nicotinamide mononucleotide (NMNH) potently enhances NAD^+ and suppresses glycolysis, the TCA cycle, and cell growth. *Journal of Proteome Research*, **20**(5): 2596–2606.

Mani S, Srivastava V, Shandilya C, et al. 2024. Mitochondria: the epigenetic regulators of ovarian aging and longevity. *Frontiers in Endocrinology*, **15**: 1424826.

Marcouiller F, Jochmans-Lemoine A, Ganouna-Cohen G, et al. 2021. Metabolic responses to intermittent hypoxia are regulated by sex and estradiol in mice. *American Journal of Physiology-Endocrinology and Metabolism*, **320**(2): E316–E325.

Mclaughlin EA, Mciver SC. 2009. Awakening the oocyte: controlling primordial follicle development. *Reproduction*, **137**(1): 1–11.

Miao YL, Chen JY, Gao Q, et al. 2021. Generation and assessment of high-quality mouse oocytes and embryos following nicotinamide mononucleotide administration. *STAR Protocols*, **2**(1): 100298.

Miao YL, Cui ZK, Gao Q, et al. 2020. Nicotinamide mononucleotide supplementation reverses the declining quality of maternally aged oocytes. *Cell Reports*, **32**(5): 107987.

Miao YL, Cui ZK, Zhu XT, et al. 2022. Supplementation of nicotinamide mononucleotide improves the quality of postovulatory aged porcine oocytes. *Journal of Molecular Cell Biology*, **14**(4): mjac025.

Nadeeshani H, Li JY, Ying TL, et al. 2022. Nicotinamide mononucleotide (NMN) as an anti-aging health product - Promises and safety concerns. *Journal of Advanced Research*, **37**: 267–278.

Newby EA, Myers DA, Ducsay CA. 2015. Fetal endocrine and metabolic adaptations to hypoxia: the role of the hypothalamic-pituitary-adrenal axis. *American Journal of Physiology-Endocrinology and Metabolism*, **309**(5): E429–E439.

Noh H, Sen Gupta S, Seshadri S, et al. 2026. NMN supplementation as a strategy to improve oocyte quality: a systematic review and transcriptomic analysis. *Journal of Assisted Reproduction and Genetics*, **43**(1): 51–65.

Okabe K, Yaku K, Tobe K, et al. 2019. Implications of altered NAD metabolism in metabolic disorders. *Journal of Biomedical Science*, **26**(1): 34.

Okoye CN, Koren SA, Wojtovich AP. 2023. Mitochondrial complex I ROS production and redox signaling in hypoxia. *Redox Biology*, **67**: 102926.

Osmond C, Barker DJ. 2000. Fetal, infant, and childhood growth are predictors of coronary heart disease, diabetes, and hypertension in adult men and women. Environmental Health Perspectives, 108(Suppl 3): 545–553.

Pi HF, Xu SC, Reiter RJ, et al. 2015. SIRT3-SOD2-mROS-dependent autophagy in cadmium-induced hepatotoxicity and salvage by melatonin. *Autophagy*, **11**(7): 1037–1051.

Ramírez-Martín N, Buigues A, Rodríguez-Varela C, et al. 2025. Nicotinamide mononucleotide supplementation improves oocyte developmental competence in different ovarian damage conditions. American Journal of Obstetrics and Gynecology, 233(2): 112. e1–112. e20.

Shiratsuki S, Hara T, Munakata Y, et al. 2016. Low oxygen level increases proliferation and metabolic changes in bovine granulosa cells. *Molecular and Cellular Endocrinology*, **437**: 75–85.

Simon MC, Keith B. 2008. The role of oxygen availability in embryonic development and stem cell function. *Nature Reviews Molecular Cell Biology*, **9**(4): 285–296.

Simonson TS, Yang YZ, Huff CD, et al. 2010. Genetic evidence for high-altitude adaptation in Tibet. *Science*, **329**(5987): 72–75.

Soltani A, Salmaninejad A, Jalili-Nik M, et al. 2019. 5'-Adenosine monophosphate-activated protein kinase: a potential target for disease prevention by curcumin. *Journal of Cellular Physiology*, **234**(3): 2241–2251.

Soma M, Lalam SK. 2022. The role of nicotinamide mononucleotide (NMN) in anti-aging, longevity, and its potential for treating chronic conditions. *Molecular Biology Reports*, **49**(10): 9737–9748.

Song MJ, Li Y, Zhou YH, et al. 2022. Nicotinamide mononucleotide

supplementation improves the quality of porcine oocytes under heat stress. *Journal of Animal Science and Biotechnology*, **13**(1): 68.

Tatone C, Di Emidio G, Barbonetti A, et al. 2018. Sirtuins in gamete biology and reproductive physiology: emerging roles and therapeutic potential in female and male infertility. *Human Reproduction Update*, **24**(3): 267–289.

Tatone C, Di Emidio G, Vitti M, et al. 2015. Sirtuin functions in female fertility: possible role in oxidative stress and aging. *Oxidative Medicine and Cellular Longevity*, **2015**: 659687.

Vargas Á, Bustos-Obregón E, Hartley R. 2011. Effects of hypoxia on epididymal sperm parameters and protective role of ibuprofen and melatonin. *Biological Research*, **44**(2): 161–167.

Vo KCT, Sato Y, Kawamura K. 2023. Improvement of oocyte quality through the SIRT signaling pathway. *Reproductive Medicine and Biology*, **22**(1): e12510.

Wang JJ, Yu XW, Wu RY, et al. 2018. Starvation during pregnancy impairs fetal oogenesis and folliculogenesis in offspring in the mouse. *Cell Death & Disease*, **9**(5): 452.

Wang YH, Hao YJ, Zhang H, et al. 2020. DNA hypomethylation of miR-30a mediated the protection of hypoxia postconditioning against aged cardiomyocytes hypoxia/reoxygenation injury through inhibiting autophagy. *Circulation Journal*, **84**(4): 616–625.

Wu H, Zhao XF, Hochrein SM, et al. 2023. Mitochondrial dysfunction promotes the transition of precursor to terminally exhausted T cells through HIF-1α-mediated glycolytic reprogramming. *Nature Communications*, **14**(1): 6858.

Zhang L, Han LS, Ma RJ, et al. 2015. Sirt3 prevents maternal obesity-associated oxidative stress and meiotic defects in mouse oocytes. *Cell Cycle*, **14**(18): 2959–2968.

Zhang LY, Jia GX, Tao HP, et al. 2025a. Maternal hypoxia exposure perturbs imprinted gene methylation in adult sperm and induces intergenerational placental impairments in male offspring. *Zoological Research*, **46**(6): 1273–1288.

Zhang LY, Liu KX, Liu ZQ, et al. 2024a. In pre-clinical study fetal hypoxia caused autophagy and mitochondrial impairment in ovary granulosa cells mitigated by melatonin supplement. *Journal of Advanced Research*, **64**: 15–30.

Zhang LY, Wang ZC, Lu TF, et al. 2020. Mitochondrial Ca^{2+} overload leads to mitochondrial oxidative stress and delayed meiotic resumption in mouse oocytes. *Frontiers in Cell and Developmental Biology*, **8**: 580876.

Zhang LY, Zhang K, Zhao X, et al. 2024b. Fetal hypoxia exposure induces Hif1a activation and autophagy in adult ovarian granulosa cells. *Biology of Reproduction*, **111**(6): 1220–1234.

Zhang Q, Ren J, Wang FF, et al. 2022. Mitochondrial and glucose metabolic dysfunctions in granulosa cells induce impaired oocytes of polycystic ovary syndrome through Sirtuin 3. *Free Radical Biology and Medicine*, **187**: 1–16.

Zhang T, Xi QS, Wang D, et al. 2019a. Mitochondrial dysfunction and endoplasmic reticulum stress involved in oocyte aging: an analysis using single-cell RNA-sequencing of mouse oocytes. *Journal of Ovarian Research*, **12**(1): 53.

Zhang WH, Zhang JM, Xue HX, et al. 2024c. Nicotinamide mononucleotide improves endometrial homeostasis in a rat model of polycystic ovary syndrome by decreasing insulin resistance and regulating the glylytic pathway. *Molecular Nutrition & Food Research*, **68**(21): 2400340.

Zhang XB, Cai JH, Yang YY, et al. 2019b. Telmisartan attenuates kidney apoptosis and autophagy-related protein expression levels in an intermittent hypoxia mouse model. *Sleep and Breathing*, **23**(1): 341–348.

Zhang Y, Ai C, Huang FZ, et al. 2025b. β-Nicotinamide mononucleotide blocks UVB-induced collagen reduction via regulation of ROS/MAPK/AP-1 and stimulation of mitochondrial proline biosynthesis. *Photochemical & Photobiological Sciences*, **24**(2): 293–306.

Zhang Y, Bai J, Cui ZK, et al. 2023. Polyamine metabolite spermidine rejuvenates oocyte quality by enhancing mitophagy during female reproductive aging. *Nature Aging*, **3**(11): 1372–1386.

Zhao HC, Ding T, Ren Y, et al. 2016. Role of Sirt3 in mitochondrial biogenesis and developmental competence of human in vitro matured oocytes. *Human Reproduction*, **31**(3): 607–622.

Zhao LH, Lu TF, Gao L, et al. 2017. Enriched endoplasmic reticulum-mitochondria interactions result in mitochondrial dysfunction and apoptosis in oocytes from obese mice. *Journal of Animal Science and Biotechnology*, **8**: 62.

Zhou J, Qian CY, Tong RQ, et al. 2018. Hypoxia induces apoptosis of mouse spermatocyte GC-2 cells through activation of autophagy. *Cell Biology International*, **42**(9): 1124–1131.